Geophysical Journal International

Two-phase dynamics of volcanic eruptions: compaction, compression and the conditions for choking

David Bercovici[1] and Chloé Michaut[2]

[1]*Department of Geology and Geophysics, Yale University,* PO Box 208109, *New Haven, CT* 06520-8109, *USA. E-mail: david.bercovici@yale.edu*
[2]*Institut de Physique du Globe Paris, Université Paris Diderot, Laboratoire de Géophysique Spatiale et Planétaire* 4, *Av. de Neptune,* 94107 *St Maur des Fossés, France*

SUMMARY
Volcanic eruptions involve high-speed turbulent flows of gas and magma mixtures in which peak gas velocities often approach 600 m s^{-1}. Such speeds are well in excess of the slow mixture sound speeds of approximately 150 m s^{-1} predicted by pseudo-gas theory, in which the gas and magma phases are assumed to be locked to each other; eruptions thus appear to be highly super-sonic. Indeed, flow in the volcanic conduit will choke when it reaches the sound speed and to attain supersonic velocities one must invoke special conduit nozzle shapes. However, the pseudo-gas approximation is a long-wavelength assumption, while choking and acoustic shocks are a short-wavelength effect; thus, the approximation is likely inapplicable for the choking phenomenon. To allow for non-pseudo-gas effects, such as phase separation, in the short-wavelength limit requires a more complete treatment of two-phase eruptions. We therefore develop and explore a model for two-phase, high Reynolds number flow of a compacting suspension of magma particles in a compressible gas. Flow properties, such as mixture density, are controlled both by gas content as well as gas compressibility, both of which vary according to different processes of compaction and compression, respectively. The two phases of the mixture separate because of their different densities, and the interaction forces (turbulent drag and inertial exchange) can be complex. The model is used to examine acoustic-porosity wave propagation and the development of shocks or choking structures in a volcanic conduit. Sound waves in separable mixtures are highly dispersive with fast waves propagating at the pure gas sound speed at small wavelengths, slow waves travelling at the pseudo-gas speed at long wavelengths, and pure attenuation and sound blocking at intermediate wavelengths. As shock fronts in gas density develop they become increasingly short wavelength features and thus will only cause choking if the maximum speed in the flow reaches the pure gas sound speed. Non-linear, finite-amplitude steady-state models of eruptions in a volcanic conduit show that compaction occurs over the magma particle gravitational deceleration height, and either suppresses gas expansion for fast eruptions, or isopycnally collapses the gas volume near the base of the erupting column for slow eruptions. Once compaction ceases, the gas expands toward a shock structure or choking point, which is coincident with a rapid gas acceleration and a high-speed vent eruption. Increased turbulent drag between the gas and particles suppresses compaction effects but greatly sharpens the shock front at the choking point. Although the standard pseudo-gas models predict such choking to occur at low velocities, the full two-phase theory always has choking occur when the gas reaches the pure gas sound speed, in keeping with the sound-speed dispersion analysis. Therefore , the full two-phase theory predicts choking to occur at the pure gas sound speed, which (for water vapour at the relevant high temperatures) is about 700 m s^{-1}. Eruption velocities of 600 m s^{-1} are therefore fully consistent with the limit imposed by this choking condition, and no special conditions to obtain supersonic eruptions, such as nozzled conduit geometries, are necessary.

Key words: Non-linear differential equations; Explosive volcanism; Eruption mechanisms and flow emplacement.

GJI Mineral physics, rheology, heat flow and volcanology

1 INTRODUCTION

Volcanic eruptions are one of the more dramatic natural phenomena in planetary sciences. Mixtures of gas and magma are ejected from vents at high velocities, and can subsequently develop into a variety of eruptive forms, from plinian eruptions that eject ash and aerosol nucleating gases into the upper atmosphere, to massively destructive pyroclastic flows and *nuées ardentes*.

Explosive eruptions generally occur after vesicular magma fragments in the volcanic conduit to form a mixture of ash and pyroclasts suspended in gas. Fragmentation is followed by rapid decompression of the gas phase, which causes a large decrease in the mean mixture density and substantial acceleration of the mixture; fragmentation also marks the transition from laminar to turbulent flow in the volcanic conduit. Depending on the eruptive discharge rate and gas volume fraction, the gas–magma mixture exits the vent to form either a plinian column or a pyroclastic flow (Wilson *et al.* 1980; Woods 1995). Assumptions about the dynamics of the two-phase mixture are critical for inferring both the excess pressure and the mixture density at the exit, both of which determine the subsequent explosive regime. In particular, the facility with which phases separate and the gas escapes the mixture controls both the gas density and pressure, as well as the gas volume fraction (i.e. poor separability will cause the gas to become trapped and over-pressured). Therefore, the two-phase physics of the turbulent mixture in the volcanic conduit determines the nature of the eventual explosive eruption.

Flow models for volcanically eruptive mixtures frequently employ the *pseudo-gas approximation*, in which the mixture acts as a single-phase medium wherein the magma and gas components at a point in space are constrained to have identical velocities (e.g. Jaupart & Tait 1990; Woods 1995). This approximation has particular importance for predicting choking conditions and hence maximum flow velocities in a conduit.

Choking occurs when flows approach the sound speed and thus cannot adjust to pressure changes in the conduit (they are 'choked' in that an increase in driving pressure causes no change in flow rate) and are associated with development of an acoustic shock or discontinuity in gas pressure and density (e.g. John 1969; Wilson *et al.* 1980; Vergniolle & Jaupart 1986). The effective sound speed in a pseudo-gas is considerably reduced from the pure gas sound speed (see Drew & Passman 1999, chap. 22); this occurs because incompressibility of the mixture is dictated by the gas, but inertia is determined by the mean mixture density. Pseudo-gas models thus predict choking to occur at relatively low velocities, and in volcanic conduits between 100 and 200 m s^{-1}. However, the exit velocity of gas in eruptions have been estimated to be as high as 600 m s^{-1} (Wilson 1976; Wilson *et al.* 1980), which is comparable to the sound speed of the pure gas phase (primarily water vapour) at conduit temperatures of order 1000 K, and is much larger than the effective sound speed in a pseudo-gas mixture (Kieffer 1977). If the choking condition is dictated by the reduced mixture sound speed, then reaching velocities as high as 600 m s^{-1} is problematic because such speeds would be nominally supersonic. This 'slow choking' paradox is typically circumvented by appealing to nozzle effects in the conduit (Wilson *et al.* 1980; Mitchell 2005) wherein a narrow throat—as in the classic de Laval or converging-diverging jet nozzle (John 1969)—permits super-sonic velocities down stream of the choking point, which occurs at the throat. However, choking at the reduced pseudo-gas sound speed is itself a questionable assumption because the pseudo-gas model is a long-wavelength approximation (Drew & Passman 1999), whereas acoustic shocks and choking are by definition short wavelength effects.

If the phases separate, the choking condition is changed and the flow is significantly modified (e.g. Vergniolle & Jaupart 1986; Kozono & Koyaguchi 2009a,b). For example, Vergniolle & Jaupart (1986) show that in a vesiculated magma, 'compound choking' of the combined flow of magma and gas bubbles occurs when the sound velocity is reached in the phase with the lowest sound speed, which is generally for the gas phase. As shown in this study, allowing for phase interactions and separation reveals that two-phase sound-waves are highly dispersive (i.e. sound-speed is dependent on wave length or frequency) and attenuated; thus, shock conditions are more varied and complex than would be implied by the pseudo-gas or other simplifications.

The effectiveness of fragmentation also plays an important role in the dynamics and velocities of conduit eruption, and thus on the stability of the eruption column and its explosive regime (pyroclastic or plinian). Indeed, fragmentation produces a broad range of magma particle sizes, from micrometer ashes to metre-sized blocks (e.g. Walker 1980; Kaminski & Jaupart 1998). Particle size strongly influences the interaction between phases and thus the separation of magma and gas as well as entrainment and heating of ambient atmosphere. In particular, smaller and lighter particles are more readily carried by the gas phase than larger, heavier magma fragments. For example, in their shock-tube experiments, Chojnicki *et al.* (2006) observe that particle velocities decrease with increasing particle size—implying reduced coupling to the gas— and are slower than that predicted by the pseudo-gas approximation [see Ogden & Wohletz (2010) for how particle size also influences shock development].

In this paper, we develop and explore a theory for the dynamics of a turbulent mixture of continuous gas and dispersed magma particles, starting at the fragmentation level. The model allows for phase interaction and separation, which leads to a variety of important effects, such as gravitational settling and compaction interacting with gas compression, as well as simultaneous acoustic and porosity waves. Acoustic waves in particular are highly dispersive, with sound speeds and attenuation that depend strongly on wavelength and/or inter-phase drag. The maximum available sound speed determines the choking condition (i.e. the maximum flow velocity that can be reached before a shock develops). Non-linear calculations show that compaction and separation of the magma component under gravity can have a significant effect on eruptions, such as delaying gas expansion during lofting. Once gravitational compaction ceases, gas decompression can be very rapid and lead to high-speed eruptions that approach the gas sound speed. This rapid decompression is associated with a true choking point that is limited by the gas sound speed, not the mixture sound speed. Finally, at the choking point, the large turbulent inter-phase stresses, and the precipitous drop in gas pressure, can induce secondary fragmentation by rupturing larger particles, especially if they have significant surface roughness and trapped gas bubbles.

2 TWO-PHASE GAS DYNAMICS: THEORY

Two-phase physics has been treated extensively in the geophysics literature, most notably for viscous flows in partially molten magmas, in particular the seminal work of McKenzie (1984) (see also Spiegelman 1993). Low viscosity and turbulent two-phase flows in volcanic eruptive systems have been developed largely for

1-D steady-state systems following the work of Wallis (1969), and employ various simplifying and empirical assumptions about inter-phase drag and interactions (e.g. Vergniolle & Jaupart 1986; Papale 2001; Kozono & Koyaguchi 2009a).

The general physics of multi-phase, low viscosity, turbulent flows, however, is in itself a broad and extremely rich field (e.g. Crowe *et al.* 1998; Drew & Passman 1999). Given the complexity of such flows there is no single, generally accepted theory, and most of the problems plaguing these theories reside not just in classical turbulence closure, but also in the multiple interactions between phases at their interface. Nevertheless, general continuum theories have been developed with averaged equations (e.g. Zhang & Prosperetti 1994) following the formalism of Drew (1971, 1983), Drew & Segel (1971), Drew & Passman (1999). The continuum approach has, for example, been employed in 2- and 3-D numerical models of flows with gas compressibility effects (e.g. Venkateswaran *et al.* 2002), and chemical reactions between components in combustion dynamics (e.g. Pitsch 2006); lagrangian numerical modelling has also been used to approach the motion of dispersed particles in a turbulent continuous phase (see Crowe *et al.* 1996, 1998).

The focus of this paper is on two-phase flows in jets and conduits, with attention to acoustic wave propagation, shock development and choking. Past modelling of multi-component or multi-phase turbulent jets and plumes has been the subject of the simplified classical entrainment formalism of Morton *et al.* (1956), with extensions into more general two-phase treatment (Melville & Bray 1979) and applications to volcanic eruptions (Woods 1988). Studies of propagation of acoustic waves in two-phase media have examined the classic reduction of sound speed in a pseudo-gas (see Drew & Passman 1999, chap. 22), sound generated by bubble vibration (Crighton & Williams 1969; Drew & Passman 1999, chap. 22), and dispersion of waves in water vapour caused by thermal equilibration (Young & Guha 1991) (which we assume to be negligible here; see Appendix B). The slow propagation of acoustic shock fronts in liquids with bubbles is a classical subject dating to the work of Campbell & Pitcher (1958), as is the mixing shock in which flows with dispersed liquid particles transition abruptly to a foam structure (Witte 1969); see also review in Drew & Passman (1999, chap. 22). Acoustic shocks are well known to form when gas rapidly expands on exiting a diverging nozzle (John 1969), as has been applied for volcanic eruptions exiting through vents or craters (e.g. Wilson 1976; Woods & Bower 1995; Mitchell 2005). Choking conditions inside a conduit due to gas expanding on ascent through lower lithostatic or hydrostatic pressures has been treated with steady-state models (e.g. Vergniolle & Jaupart 1986; Kozono & Koyaguchi 2009a). However, here we seek to examine how acoustic waves in the conduit are affected by phase separation, compaction, compression and turbulent drag, and how the resultant variations in sound speed influence shock development and choking. To that end, we briefly develop a general continuum theory for high-velocity two-phase volcanic flows by building on some of the recent formalism established by Bercovici *et al.* (2001a,b), Ricard *et al.* (2001), Bercovici & Ricard (2003) and many of the subsequent papers (e.g. Ricard & Bercovici 2003; Bercovici & Ricard 2005; Hier-Majumder *et al.* 2006; Sramek *et al.* 2007; Landuyt *et al.* 2008; Michaut & Bercovici 2009; Michaut *et al.* 2009). We introduce several new features for this extended theory, such as gas compressibility, turbulent drag and inertial exchange between phases, which differ from previous general treatments (Appendix A).

2.1 Mass conservation

Treatments of mass conservation in two-phase dynamics are rather standard, although here we consider gas compressibility and thus solve for gas density, which changes subject to changes in pressure and temperature as prescribed by an ideal gas law. The equations involving the mass transport of the continuous gas and dispersed magma/ash phases are thus

$$\frac{\partial \rho_g \phi}{\partial t} + \nabla \cdot [\rho_g \phi \mathbf{v}_g] = 0, \tag{1}$$

$$\frac{\partial (1-\phi)}{\partial t} + \nabla \cdot [(1-\phi)\mathbf{v}_m] = 0, \tag{2}$$

where ϕ is gas volume fraction, ρ_g is gas density, $\mathbf{v}_g$ and $\mathbf{v}_m$ are the gas and magma velocities, respectively. We have assumed that the magma is incompressible thus ρ_m is a constant, and that there is no exchange of mass between phases (i.e. gas exsolution is negligible after fragmentation). The ideal gas law is used for an equation of state for the gas density wherein

$$\rho_g = \frac{P_g m_g}{RT} \tag{3}$$

in which P_g is gas pressure, m_g is the gas molar mass, T is temperature (the magma and gas are assumed to be in local thermodynamic equilibrium and thus at the same temperature) and R is the gas constant. Relations for gas pressure and temperature are necessarily developed through conservation of momentum and energy equations.

2.2 Momentum conservation

For the particular application of volcanic eruptions, we must consider acceleration and inertia of both phases, the gas being a low viscosity fluid and the magma being in the form of suspended particles so that there is no viscous matrix stress (i.e. the particle contact is assumed negligible). The momentum equations for each phase are

$$\rho_g \phi \frac{D_g \mathbf{v}_g}{Dt} = -\phi \left[\nabla P_g + \rho_g g \hat{\mathbf{z}} \right] + \Delta \boldsymbol{I} + \omega \left[\Delta P \nabla \phi + \nabla (\sigma \Theta) \right] \tag{4}$$

$$\rho_m (1-\phi) \frac{D_g \mathbf{v}_m}{Dt} = -(1-\phi) \left[\nabla P_m + \rho_m g \hat{\mathbf{z}} \right] - \Delta \boldsymbol{I} + (1-\omega) \left[\Delta P \nabla \phi + \nabla (\sigma \Theta) \right], \tag{5}$$

where g is gravity, P_m is magma pressure, $\Delta P = P_m - P_g$, surface tension is σ and ω is a coefficient for how surface tension partitions between phases, that is to what extent it is more embedded in one phase than the other (Bercovici & Ricard 2003). The material derivatives with respect to each phase are

$$\frac{D_g}{Dt} = \frac{\partial}{\partial t} + \mathbf{v}_g \cdot \nabla, \qquad \frac{D_m}{Dt} = \frac{\partial}{\partial t} + \mathbf{v}_m \cdot \nabla. \tag{6}$$

Moreover, Θ is the interfacial area per unit volume. Surface tension might play a role in keeping magma particles coherent but, as the particles are assumed to have negligible contact, it plays little role in driving capillary flow or fusion of magma particles. Given negligible surface tension effects, and the lack of viscous matrix stresses, we can assume the pressure difference $\Delta P = 0$, and thus there is only one relevant pressure P_g (see also Appendix B).

$\Delta \boldsymbol{I}$ is the interaction force between phases only due to flow (the pressure difference and surface tension interaction have already been isolated and result in the terms proportional to ω), and is thus associated with viscous and turbulent Darcy drag (for flow through a permeable matrix) or Stokes drag (for motion of non-connected parcels of one phase through the other), as well as inertial exchange from one phase accelerating through the other. This interaction force is discussed in detail in Appendix A in which we propose the net interaction force

$$\Delta \boldsymbol{I} = c\Delta\mathbf{v} + \frac{1}{2}\check{\rho}\left(\frac{\partial\Delta\mathbf{v}}{\partial t} + \check{\mathbf{v}}\cdot\nabla\Delta\mathbf{v}\right). \tag{7}$$

The coefficient c is associated with Darcy or Stokes drag, which in a turbulent mixture of dispersed particles takes the form

$$c = \bar{c}(1-\phi)(1+\Gamma|\Delta\mathbf{v}|), \tag{8}$$

where for particles of size r moving through gas of viscosity μ_g, the parameters $\bar{c} \sim \mu_g/r^2$ and $\Gamma \sim \rho_g r/\mu_g$ govern laminar and turbulent drag, respectively (Appendix A). The quantities $\check{\mathbf{v}}$ and $\check{\rho}$ are effective interface velocity and density (see Appendix A and in particular eqs A10 and A12).

2.3 Energy conservation summary

Energy conservation is developed in detail in Appendix B, where we show that in the absence of substantial frictional heating due to phase separation, the eruption is largely isentropic, in which case the energy equation becomes

$$\frac{D_g}{Dt}\log\left(\frac{T}{\rho_g^{2/\nu}}\right) + \frac{(1-\phi)\rho_m c_m}{\phi c_g \rho_g}\frac{D_m\log T}{Dt} = 0, \tag{9}$$

where T is temperature, c_m and c_g are specific heats of magma and gas and ν is the number of degrees of freedom (e.g. 3 for monatomic gas, 5 for diatomic, etc.).

In the post-fragmentation eruption column, the gas fraction ϕ is significant and thus ϕ is comparable to 1. However, $\rho_m \gg \rho_g$ (and the heat capacities are of comparable magnitude) thus the second term on the left side of (9) dominates (unless $\phi \to 1 - \rho_g/\rho_m$ such that the mixture becomes at least 99 per cent gas by volume), which means that the eruption is predominantly isothermal; that is the temperature is buffered by the large heat capacity per volume ($\rho_m c_m$) of the magma. Therefore, we will assume that the system is predominantly isothermal and temperature T is hereafter a constant.

3 GENERAL 1-D MODEL

Basic two-phase eruption dynamics in a volcanic conduit can be treated by the 1-D version of the theory. Conduit wall drag is not explicitly included because, in 1-D, it adds terms comparable in form but smaller in magnitude to interphase drag (Michaut *et al.* 2009), which is examined over a wide parameter range anyway. Our goal is to infer the interaction between phase separation, mixture compaction and gas decompression, and how these processes influence eruption dynamics, shock development and choking conditions.

3.1 Governing equations

The general 1-D governing equations are extracted from (1), (2), (4) and (5) with (7). As discussed earlier, we assume there is no surface tension and thus there is only one pressure P_g for the whole mixture, and that the system is predominantly isothermal and thus T is fixed. Pressure is thus only a function of gas density and thus

$$dP_g = \frac{dP_g}{d\rho_g}d\rho_g = \mathcal{C}_g^2 d\rho_g \tag{10}$$

where

$$\mathcal{C}_g = \sqrt{RT/m_g} \tag{11}$$

is the gas sound speed (eq. 3). With these assumptions, the 1-D governing equations become

$$\frac{\partial(\rho_g\phi)}{\partial t} + \frac{\partial(\rho_g\phi w_g)}{\partial z} = 0, \tag{12}$$

$$\frac{\partial(1-\phi)}{\partial t} + \frac{\partial[(1-\phi)w_m]}{\partial z} = 0, \tag{13}$$

$$\rho_g\phi\left(\frac{\partial w_g}{\partial t} + w_g\frac{\partial w_g}{\partial z}\right) = -\phi\mathcal{C}_g^2\frac{\partial\rho_g}{\partial z}$$
$$-\rho_g\phi g + c\Delta w + \frac{1}{2}\check{\rho}\left(\frac{\partial\Delta w}{\partial t} + \check{w}\frac{\partial\Delta w}{\partial z}\right), \tag{14}$$

$$\rho_m(1-\phi)\left(\frac{\partial w_m}{\partial t} + w_m\frac{\partial w_m}{\partial z}\right) = -(1-\phi)\mathcal{C}_g^2\frac{\partial\rho_g}{\partial z}$$
$$-\rho_m(1-\phi)g - c\Delta w - \frac{1}{2}\check{\rho}\left(\frac{\partial\Delta w}{\partial t} + \check{w}\frac{\partial\Delta w}{\partial z}\right), \tag{15}$$

where w_g, w_m and $\check{w}$ are the vertical components of the velocity vectors $\mathbf{v}_g$, $\mathbf{v}_m$ and $\check{\mathbf{v}}$ (see Appendix A and in particular eq. A10). The four governing eqs (12)–(15) are sufficient to determine ϕ, ρ_g, w_g and w_m, given suitable boundary conditions.

3.2 Physical properties and scales

The physical setting for the model is a volcanic conduit, between the depths associated with fragmentation and the vent, which is typically over length scales of several 100 m to at most a few kilometres. Estimates of pressure at fragmentation comes from modelling and geochemistry data; modelling shows that pressure at fragmentation depends on gas content and overpressure in the chamber, and is typically 10–50 MPa (Massol & Jaupart 1999; Melnik 2000; Kozono & Koyaguchi 2009a). Barometric studies on microlite compositions and water content in glass inclusions give quantitative estimates for the pressure at which microlites last crystallized, and thus provide upper limits for the pressure at fragmentation; these pressure values are typically about 80–150 MPa for explosive eruptions (Blundy & Cashman 2001). We thus assume pressures reach 20–30 MPa right after fragmentation, and hence gas density at this point (with temperature $T \approx 1300$ K, and gas primarily composed of water) is 30–50 kg m^{-3}. Near the top of the vent, assuming the mixture is still over-pressured to drive the eruption (Ogden *et al.* 2008a,b) to values of order 1 MPa, and that the temperature has changed little, then the density is of approximately 2 kg m^{-3}. As shown below, an important dimensionless parameter is β_m, the ratio of magma density $\rho_m \approx 2500$ kg m^{-3} to reference gas density ρ_0; thus, β_m is of order 100 near the fragmentation point, and can increase to order 1000 near the vent.

The gas volume fraction ϕ is assumed to be large, ranging from 0.7 at the fragmentation point (Sparks 1978; Kaminski & Jaupart 1998) to close to 1 when gas expands rapidly near the vent. See Table 1 for a summary of dimensional properties of the system.

Table 1. Dimensional properties.

Name	Definition	Value or range used
ρ_m	Magma density	2500 kg m^{-3}
ρ_o	Reference/basal value of gas density, ρ_g	$2\text{–}30 \text{ kg m}^{-3}$
μ_g	Gas viscosity	10^{-5} Pa s
r	Magma particle size	$10^{-2}\text{–}10^{-4} \text{ m}$
g	Gravity	10 m s^{-2}
$\mathcal{C}_g$	Gas sound speed	700 m s^{-1}
$\mathcal{C}_\psi$	Pseudo-gas sound speed; see eq. (27)	$\sim 150 \text{ m s}^{-1}$
$\mathcal{W}_0$	Initial eruption speed	$5\text{–}50 \text{ m s}^{-1}$
$|\Delta w_0|$	Background phase separation speed; see eq. (C11)	$0.2\text{–}10 \text{ m s}^{-1}$

The gas viscosity μ_g appears in the inter-phase drag relations and, at the relevant temperatures and for water vapour, is of order 10^{-5} Pa s (Kaye & Laby 1972). Particle size r also influences drag between phases; while particles in an eruption can range from micrometre size ash to metre-sized blocks (e.g. Walker 1980; Kaminski & Jaupart 1998), we constrain our size range to 10^{-4} m $\leq r \leq 10^{-2}$ m (i.e. from 100 μm to 1 cm) because extremely fine particles are tightly coupled to the gas phase and contribute little to phase separation, whereas block-size particles are beyond the continuum assumption of two-phase theory.

Gas sound speed is given by eq. (11) and at $T \approx 1000\text{–}1300$ K, and primarily water vapour ($m_g = 18 \times 10^{-3}$ kg mol^{-1}) we find $\mathcal{C}_g \approx 700$ m s^{-1}. The ejection velocities after fragmentation are typically of order 5–50 m s^{-1} (Massol & Jaupart 1999; Kozono & Koyaguchi 2009a) and thus the gas sound speed is typically 10–100 times the post fragmentation velocity (this ratio is employed in Section 5 and is referred to by the variable $\bar{\alpha}$). As shown in Appendix C1.1, the relative velocity between phases due to gravitational separation is typically between 20 cm s^{-1} to 10 m s^{-1} (depending on particle size); thus, the sound speed is typically of order 100–1000 times the separation velocity (this ratio is employed in Section 4.2 and is referred to as α).

4 ACOUSTIC-POROSITY WAVES

Shock development and choking occurs when eruption velocities approach the speeds of acoustic waves in the mixture. Acoustic waves in volcanic mixtures are frequently treated with the pseudo-gas approximation wherein the component's velocities are assumed to be the same. Although this assumption is valid in limited types of two-phase media such as foams, the phases are generally separable and, given their different densities and inertia, will respond differently to the same pressure gradients or body forces. Sound waves in a pseudo-gas are non-dispersive and non-attenuating, and simply display wave speed reduction, depending on the mixture ratio and density contrast of components. Sound waves in a separable two-phase mixture, however, can be relatively complex, displaying both strong dispersion and attenuation. Here we illustrate the effect on acoustic waves when phase separation is permitted. First, we examine the simple case for waves in an erupting jet in zero-gravity, which by a Galilean transformation is equivalent to waves in a static column. Secondly, we examine the coupled acoustic and porosity waves in an eruption in the presence of gravity, which induces both gas decompression as well as gravitational separation of phases.

4.1 Acoustic-porosity waves in a zero-gravity jet

To infer the effect of phase-separation on acoustic waves in the simplest setting, we first consider the propagation of infinitesimal

perturbations against a uniform jet in zero gravity. The jet has a given zeroth order velocity $\mathcal{W}_0$ that, because of the absence of body forces, is constant. The system of equations is Galilean invariant and can be transformed to a frame of reference travelling with the jet at velocity $\mathcal{W}_0$; in this frame the basic state is stationary. Therefore, one can linearize the dependent variables according to

$$\phi = \phi_0 + \epsilon\phi_1,$$
$$\rho_g = \rho_0(1 + \epsilon\theta_1),$$
$$w_m = \epsilon w_{m1},$$
$$w_g = \epsilon w_{g1}, \tag{16}$$

where $\epsilon \ll 1$, in which case the general 1-D time-dependent governing eqs (12)–(15) become to first order in ϵ

$$\phi_0 \frac{\partial\theta_1}{\partial t} + \frac{\partial\phi_1}{\partial t} + \phi_0 \frac{\partial w_{g1}}{\partial z} = 0, \tag{17}$$

$$\frac{\partial\phi_1}{\partial t} - (1 - \phi_0)\frac{\partial w_{m1}}{\partial z} = 0, \tag{18}$$

$$\rho_0\phi_0 \frac{\partial w_{g1}}{\partial t} = -\rho_0\phi_0\mathcal{C}_g^2 \frac{\partial\theta_1}{\partial z}$$
$$+ \bar{c}(1 - \phi_0)\Delta w_1 + \frac{1}{2}\breve{\rho}_0 \frac{\partial\Delta w_1}{\partial t}, \tag{19}$$

$$\rho_m(1 - \phi_0)\frac{\partial w_{m1}}{\partial t} = -\rho_0(1 - \phi_0)\mathcal{C}_g^2 \frac{\partial\theta_1}{\partial z}$$
$$- \bar{c}(1 - \phi_0)\Delta w_1 - \frac{1}{2}\breve{\rho}_0 \frac{\partial\Delta w_1}{\partial t}, \tag{20}$$

where $\Delta w_1 = w_{m1} - w_{g1}$, $\breve{\rho}_0$ is given by (A12) (evaluated for $\phi = \phi_0$ and $\rho_g = \rho_0$), and we have used the definition for c given by eq. (8) but with the turbulent drag term (proportional to Γ) neglected since that term is of order ϵ^2. The governing equations can be recast to elucidate bulk motion and separation by using $\overline{w}_1 = \phi_0 w_{g1} + (1 - \phi_0)w_{m1}$ to write $w_{g1} = \overline{w}_1 - (1 - \phi_0)\Delta w_1$ and $w_{m1} = \overline{w}_1 + \phi_0\Delta w_1$. With these substitutions, and subtracting eq. (18) from eq. (17) we obtain

$$\phi_0 \frac{\partial\theta_1}{\partial t} + \frac{\partial\overline{w}_1}{\partial z} = 0. \tag{21}$$

Likewise adding $\phi_0 \times$ (18) to $(1 - \phi_0)\times$(17) yields

$$\phi_0(1 - \phi_0)\frac{\partial\theta_1}{\partial t} + \frac{\partial\phi_1}{\partial t} - \phi_0(1 - \phi_0)\frac{\partial\Delta w_1}{\partial z} = 0. \tag{22}$$

Similarly adding the momentum equations (19) and (20) yields

$$\overline{\rho}_0 \frac{\partial\overline{w}_1}{\partial t} + \phi_0(1 - \phi_0)\Delta\rho_0 \frac{\partial\Delta w_1}{\partial t} = -\rho_0\mathcal{C}_g^2 \frac{\partial\theta_1}{\partial z}, \tag{23}$$

where $\Delta\rho_0 = \rho_{\mathrm{m}} - \rho_0$ and $\overline{\rho}_0 = \phi_0\rho_0 + (1-\phi_0)\rho_{\mathrm{m}}$. Finally, subtracting $(1-\phi_0)\times$ (19) from $\phi_0\times$ (20) leads to

$$\phi_0(1-\phi_0)\left(\Delta\rho_0\frac{\partial\overline{w}_1}{\partial t} + \widetilde{\rho}_0\frac{\partial\Delta w_1}{\partial t}\right) = -\overline{c}(1-\phi_0)\Delta w_1, \qquad (24)$$

where

$$\widetilde{\rho}_0 = \phi_0\rho_{\mathrm{m}} + (1-\phi_0)\rho_0 + \frac{1}{2}\frac{\rho_0\rho_{\mathrm{m}}}{\phi_0\rho_{\mathrm{m}} + (1-\phi_0)\rho_0}. \qquad (25)$$

4.1.1 Pseudo-gas approximation and acoustic speed reduction

The pseudo-gas assumption is equivalent to assuming that $\Delta w_1 = 0$. However, simply setting $\Delta w_1 = 0$ in eqs (21)–(24) leads to an over-determined set of equations (i.e. still four equations for three unknowns ϕ_1, θ_1 and $\overline{w}_1$). The pseudo-gas approximation is in fact only valid when interface drag $\overline{c}\Delta w$ is the dominant term in the momentum equation such that the phases are effectively locked together; in this case (24) becomes $\overline{c}\Delta w_1 = 0$, which is satisfied by $\Delta w_1 = 0$. The only necessary equations are then (21) and (23) for gas density perturbation θ_1 and average mixture velocity $\overline{w}_1$, which when combined lead to the wave equation

$$\frac{\partial^2\overline{w}_1}{\partial t^2} - \left(\frac{\rho_0}{\phi_0\overline{\rho}_0}\right)\mathcal{C}_{\mathrm{g}}^2\frac{\partial^2\overline{w}_1}{\partial z^2} = 0. \qquad (26)$$

The pseudo-gas acoustic wave speed

$$\mathcal{C}_\psi = \sqrt{\frac{\rho_0}{\phi_0\overline{\rho}_0}}\mathcal{C}_{\mathrm{g}} \qquad (27)$$

is the well-known reduced sound speed for mixtures (e.g. Drew & Passman 1999, chap. 22). For example, if $\phi = 0.7$ and $\beta_{\mathrm{m}} = \rho_{\mathrm{m}}/\rho_0 = 100$ (for a typical post-fragmentation gas density) then $\mathcal{C}_\psi \approx \mathcal{C}_{\mathrm{g}}/5$.

4.1.2 Waves in a zero-gravity jet with phase separation

The general wave equations including phase separation in which $\Delta w_1 \neq 0$ arise from the combination of (21) with (23), which yields

$$\frac{\partial^2\overline{w}_1}{\partial t^2} + \left(\frac{\phi_0(1-\phi_0)\Delta\rho_0}{\overline{\rho}_0}\right)\frac{\partial^2\Delta w_1}{\partial t^2} - \left(\frac{\rho_0}{\phi_0\overline{\rho}_0}\right)\mathcal{C}_{\mathrm{g}}^2\frac{\partial^2\overline{w}_1}{\partial z^2} = 0 \qquad (28)$$

and (24) which we rewrite as

$$\frac{\partial\Delta w_1}{\partial t} + \frac{\Delta\rho_0}{\widetilde{\rho}_0}\frac{\partial\overline{w}_1}{\partial t} + \frac{\overline{c}}{\phi_0\widetilde{\rho}_0}\Delta w_1 = 0. \qquad (29)$$

We specify a sinusoidal wave form in that $(\overline{w}_1, \Delta w_1) \sim \mathrm{e}^{ik(z-\mathcal{C}t)}$ where k is wavenumber and $\mathcal{C}$ is wave speed; with this assumption we arrive at the characteristic equation

$$\left(\frac{\rho_0\mathcal{C}_{\mathrm{g}}^2}{\phi_0\overline{\rho}_0} - \mathcal{C}^2\right)\left(1 + \frac{i\overline{c}}{\phi_0\widetilde{\rho}_0k\mathcal{C}}\right) + \frac{\phi_0(1-\phi_0)\Delta\rho_0^2}{\overline{\rho}_0\widetilde{\rho}_0}\mathcal{C}^2 = 0. \qquad (30)$$

If we scale wave speed according to $\mathcal{C} = \mathcal{C}_\psi\widehat{\mathcal{C}}$ (where $\mathcal{C}_\psi$ is given by eq. 27) the above characteristic equation is given simply by

$$\widehat{\mathcal{C}}(1 - \gamma\widehat{\mathcal{C}}^2) + i\lambda(1 - \widehat{\mathcal{C}}^2) = 0, \qquad (31)$$

where

$$\gamma = 1 - \frac{\Delta\rho_0^2\phi_0(1-\phi_0)}{\overline{\rho}_0\widetilde{\rho}_0}, \qquad (32)$$

$$\lambda = \frac{\overline{c}}{\phi_0\widetilde{\rho}_0\mathcal{C}_\psi k}, \qquad (33)$$

where λ accounts for both drag and wavelength.

In the limit of no interface drag where $\overline{c} = \lambda = 0$, eq. (31) leads to $\widehat{\mathcal{C}} = \pm 1/\sqrt{\gamma}$. Since $\rho_0 \ll \rho_{\mathrm{m}}$ it is easily shown that $\gamma \approx \frac{1+\phi_0}{2\phi_0}\frac{\mathcal{C}_\psi^2}{\mathcal{C}_{\mathrm{g}}^2}$ in which case the dimensional wave speed is

$$\mathcal{C} = \mathcal{C}_\psi\widehat{\mathcal{C}} \approx \pm\sqrt{\frac{2\phi_0}{1+\phi_0}}\mathcal{C}_{\mathrm{g}}. \qquad (34)$$

For $\phi_0 \to 1$, we find $\mathcal{C} \approx \pm\mathcal{C}_{\mathrm{g}}$ for unhindered phase separation with only modest wave speed reduction for smaller ϕ (unless $\phi \ll 1$, which is not appropriate for the approximations made in this study).

For the limit of very large wavelength or interface drag $\lambda \to \infty$, eq. (31) yields $\widehat{\mathcal{C}} = \pm 1$, which when redimensionalized leads to

$$\mathcal{C} = \mathcal{C}_\psi\widehat{\mathcal{C}} = \pm\mathcal{C}_\psi, \qquad (35)$$

which is the pseudo-gas solution for reduced wave speed (see Section 4.1.1).

An example of the full solution (31) is shown in Fig. 1 for a full range of values of λ displaying both the separable-phase and pseudo-gas limits. As λ increases from 0, the real part of $\widehat{\mathcal{C}}$ decreases from $\sim\mathcal{C}_{\mathrm{g}}/\mathcal{C}_\psi$ to 0 for a specific range of λ, and then increases again to 1 as $\lambda \to \infty$. In the range that $\Re(\widehat{\mathcal{C}}) = 0$ we find that $\Im(\widehat{\mathcal{C}})$ is both significant and negative which corresponds to purely decaying modes. In particular, in this range, waves are blocked, that is they do not propagate and are only attenuated. The conditions for which $\widehat{\mathcal{C}}$ is purely imaginary can be inferred by writing $\widehat{\mathcal{C}} = -i\mathcal{G}$ in which eq. (31) leads to

$$\mathcal{G}(1 + \gamma\mathcal{G}^2) - \lambda(1 + \mathcal{G}^2) = 0. \qquad (36)$$

The range of λ for which the solutions to (36) are only real (i.e. *casus irreducibilis*) correspond to a zero discriminant for the cubic equation, that is when

$$4\lambda^4 - (1 + 18\gamma - 27\gamma^2)\lambda^2 - 4\gamma = 0, \qquad (37)$$

which implies that the range of λ for which $\mathcal{G}$ is real (i.e. $\widehat{\mathcal{C}}$ is purely imaginary) is given by

$$\lambda_\pm = \sqrt{\frac{1}{8}\left(1 + 18\gamma - 27\gamma^2 \pm \sqrt{(1 + 18\gamma - 27\gamma^2)^2 - 64\gamma}\right)}. \qquad (38)$$

For $\gamma \to 0$ the range of λ is $\lambda_\pm = [0, \frac{1}{2}]$. Moreover, $\lambda_\pm$ is guaranteed real provided $(1 + 18\gamma - 27\gamma^2)^2 - 64\gamma \geq 0$; this condition is in fact equivalent to

$$(9\gamma - 1)^3(\gamma - 1) \geq 0, \qquad (39)$$

which holds for $\gamma \leq 1/9$ (as well as $\gamma \geq 1$ although this is unphysical given typical values of γ from eq. (32) for $\rho_0 \ll \rho_{\mathrm{m}}$). Thus, $\gamma = 1/9$ is the maximum γ permitting a range of λ in which $\mathcal{G}$ is real (although for $\gamma = 1/9$ this range collapses to $\lambda_\pm = 1/\sqrt{3}$). Therefore, for $0 \leq \gamma \leq 1/9$ there exist a range of λ for which sound waves are blocked. For example, as noted above, for $\beta_{\mathrm{m}} \gg 1$, $\gamma \approx \frac{1+\phi_0}{2\phi_0}\frac{\mathcal{C}_\psi^2}{\mathcal{C}_{\mathrm{g}}^2}$; for $\beta_{\mathrm{m}} = 100$ and $\phi_0 = 0.7$, $\mathcal{C}_\psi^2/\mathcal{C}_{\mathrm{g}}^2 \approx 1/21$ in which case $\gamma \approx 1/18$, which shows that a spectrum of blocked waves can exist for relevant eruption parameters.
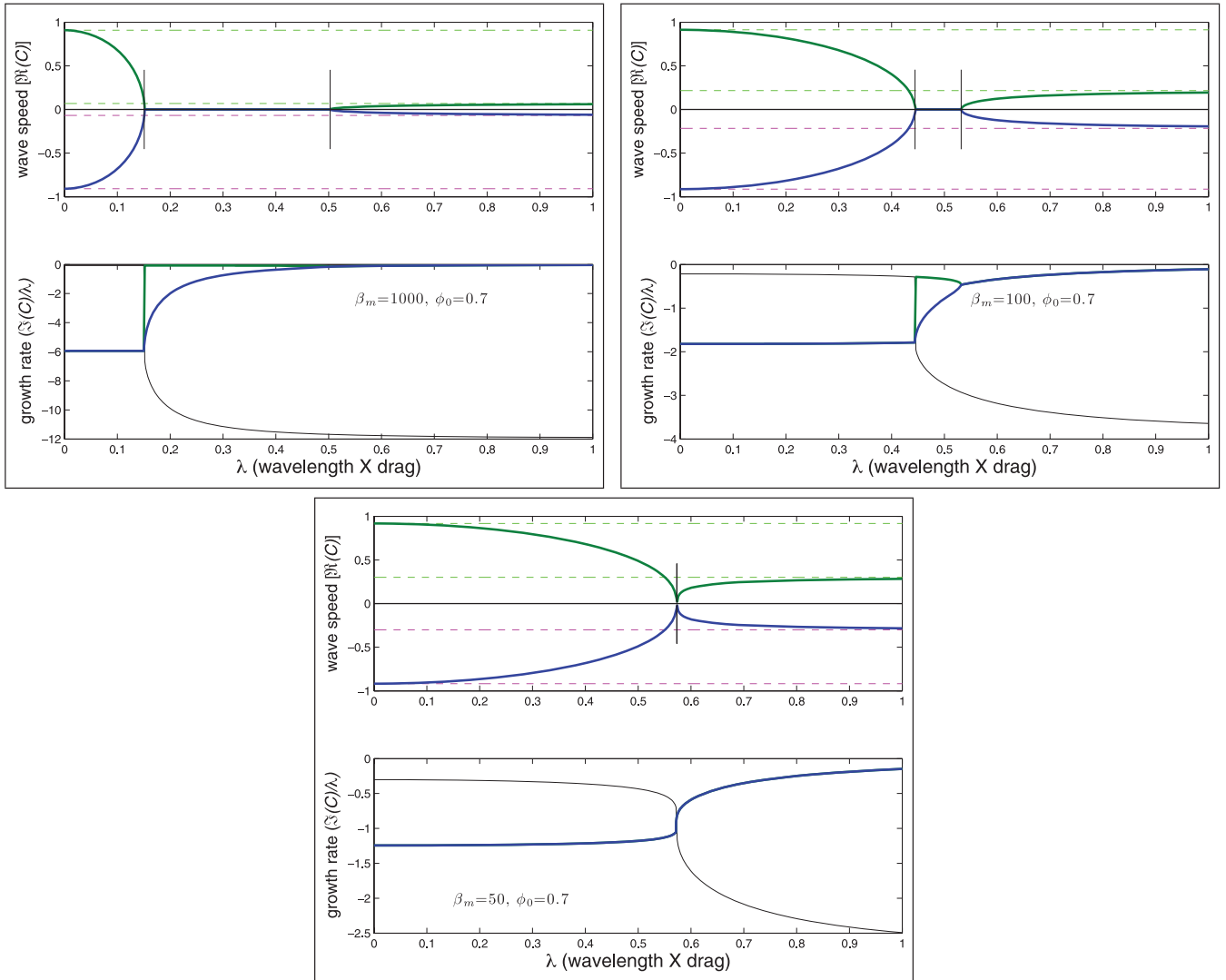
Figure 1. Acoustic-porosity wave speed for the zero-gravity jet. Shown are three cases for $\beta_m = 1000$, 100 and 50, each with $\phi_0 = 0.7$, as indicated. Dispersion curves show wave speed $\Re(\mathcal{C})$ and growth rate $\Im(\mathcal{C})/\lambda$, where here $\mathcal{C}$ is in units of gas sound speed $\mathcal{C}_g$. All three solutions to eq. (31) are displayed; green curves indicate upward propagating waves, blue are downward propagating, and the thin black lines indicate the non-propagating solutions. The dashed lines indicate asymptotes associated with normal gas sound speed (dashed lines at $\Re(\mathcal{C}) = \pm 1/\sqrt{\gamma}$) and pseudo-gas sound speed (dashed lines at $\Re(\mathcal{C}) = \pm \mathcal{C}_\psi/\mathcal{C}_g$) Vertical lines indicate upper and lower limits of λ from eq. (38) for which waves are blocked (i.e. zero sound speed and highly attenuated).

4.2 Acoustic-porosity waves in a gravitationally separating eruption

We next infer how the motion of an erupting column undergoing gravitational phase separation affects acoustic wave propagation and hence the conditions for shock development.

An eruptive column of gas–magma mixture sustains perturbations both to porosity (gas fraction) and gas density that propagate as waves. As shown in the previous section, sound waves can be much slower than the pure acoustic speed in a gas when drag between phases (or perturbation wavelengths) becomes large. In the presence of gravity, porosity waves also occur wherein pulses of high gas volume fraction are anomalously buoyant and travel faster than the ambient medium. Both types of waves exist simultaneously and can potentially interact.

We again consider the case of linear waves. Our general governing equations are (1)–(5). We assume a steady eruptive column, and consider perturbations in gas density ρ_g, porosity (gas fraction) ϕ

and velocities w_g and w_m to this steady state according to

$$\phi = \phi_0 + \epsilon \phi_1,$$
$$\rho_g = \rho_0(1 + \epsilon \theta_1),$$
$$w_m = w_{m0} + \epsilon w_{m1},$$
$$w_g = w_{g0} + \epsilon w_{g1}, \qquad (40)$$

where $\epsilon \ll 1$; the above relations are of course similar to that in the previous section (eq. 16), except here each phase has a separate background (zeroth order) velocity whose difference is Δw_0. As shown in Appendix C1, the steady-state background separation velocity is determined by the balance of gravitational segregation and turbulent inter-phase drag given by

$$\Delta w_0 = w_{m0} - w_{g0} = -\sqrt{\frac{\Delta \rho_0 g r \phi_0}{\rho_0}}, \qquad (41)$$

where r is characteristic magma particle size. As shown in Appendix C1.1, $|\Delta w_0|$ is between $20 \, \text{cm} \, \text{s}^{-1}$ and $10 \, \text{m} \, \text{s}^{-1}$.

Table 2. Dimensionless parameters.

Name	Definition	Value or range used
ϕ_0	Reference/basal gas volume fraction	0.7
β_m	Magma:gas density ratio (ρ_m/ρ_0)	100
α	Dimensionless sound-speed, Section 4.2 ($\mathcal{C}_g/\Delta w_0$)	100–1000
$\bar{\alpha}$	Dimensionless sound-speed, Section 5 ($\mathcal{C}_g/\mathcal{W}_0$)	10–100
$\mathcal{D}_0$	Laminar inter-phase drag number ($\mu_g \mathcal{W}_0/(\rho_0 r^2 g)$)	1
$\mathcal{D}_\tau$	Turbulent inter-phase drag number ($\mathcal{W}_0^2/(rg)$)	100–10000
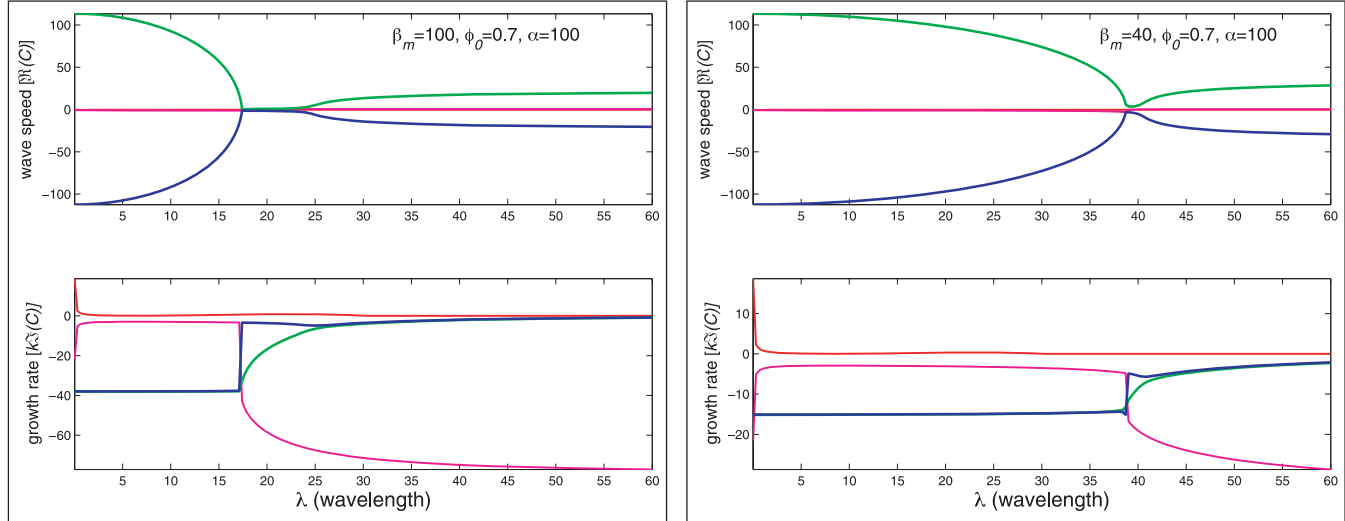
Figure 2. Wave speed for combined acoustic-porosity waves in an erupting column undergoing gravitational phase separation; from the solutions to eq. (42). Displayed are the wave speed $\Re(\mathcal{C})$ and growth-rate $k\Im(\mathcal{C})$ for four waves. Values for dimensionless parameters, namely dimensionless gas acoustic speed $\alpha = \mathcal{C}_g/|\Delta w_0|$, density ratio $\beta_m = \rho_m/\rho_0$ and background porosity (or gas volume fraction) ϕ_0, are indicated on the figure.

In the presence of gravity, the zeroth order gas density ρ_0 cannot be strictly constant; however, as also discussed in Appendix C1.1, zeroth order density gradients can be assumed small over a significant height, except when these gradients are multiplied by $\mathcal{C}_g^2$. With these assumptions of a zeroth order steady-state turbulent separation velocity, and weakly varying background gas density, we arrive at a fourth order polynomial relation for perturbation wave speed

$$\left\{ \tfrac{1}{8} k^2 (1 - 3\phi_0) \right\} \mathcal{Y}^4 - \left\{ \tfrac{1}{4} k^2 (1 - \phi_0) - ik\phi_0 (\beta_m(1 - \phi_0) + 1 \right\} \mathcal{Y}^3$$
$$+ \left\{ k^2 \left(\alpha^2 + \tfrac{1}{2} \right) \phi_0 + ik \left[\phi_0(3 - 2\phi_0) - (1 - \phi_0)\left(\beta_m \phi_0 - \tfrac{1}{2} \right) \right] \right\} \mathcal{Y}^2$$
$$- \left\{ \tfrac{1}{2} k^2 \left[4\alpha^2 \phi_0 - \tfrac{1}{2}(1 - \phi_0) \right] - 4\beta_m(1 - \phi_0)^2 \right.$$
$$\left. - ik(\phi_0[3 - 4\phi_0 - \beta_m(1 - \phi_0)]) - 4\alpha^2 \right\} \mathcal{Y}$$
$$+ k^2 \left[\left(\alpha^2 - \tfrac{1}{4} \right) \phi_0 - \tfrac{1}{8}(1 - \phi_0) \right] + 4\beta_m(1 - \phi_0)(2 - 3\phi_0)$$
$$+ ik \left[\phi_0(1 - 2\phi_0) + (1 - \phi_0)\left(\beta_m \phi_0 - \tfrac{1}{2} \right) - 4\alpha^2(2 - 3\phi_0) \right] = 0,$$

$$(42)$$

where the variable $\mathcal{Y} = 1 - (\mathcal{C} + \phi_0)/2$ and now $\mathcal{C}$ is the wave speed non-dimensionalized by $|\Delta w_0|$. The other dimensionless parameters are $\alpha = \mathcal{C}_g/|\Delta w_0|$, $\beta_m = \rho_m/\rho_0$ as defined previously, and k is the wavenumber non-dimensionalized by the $g/\Delta w_0^2$ (again, see Appendix C1). Since $0.2 \, \text{m s}^{-1} \leq |\Delta w_0| \leq 10 \, \text{m s}^{-1}$ (Appendix C1.1), then $100 \leq \alpha \leq 1000$ (see also Table 2). We also note that the reference frame for these waves is (as before)

the mean background mixture velocity of the eruptive column $\overline{w}_0 = \phi_0 w_{g0} + (1 - \phi_0)w_{m0} = \mathcal{W}_0$, which is positive.

The dispersion relation (42) has four possible solutions for the complex wave speed (Fig. 2). Two of the predicted modes are essentially identical to the simple zero-gravity acoustic modes displayed in Section 4.1.2; that is there are upward and downward propagating waves travelling at the gas sound speed at short wavelengths, and at the pseudo-gas sound speed at long wavelengths. In the current non-dimensional scheme, the simple acoustic wave speed scales as α and the pseudo-gas sound speed scales as $\alpha/\sqrt{\beta_m}$ (eq. 27). Increasing β_m widens the range of wavelengths over which slow pseudo-gas acoustic waves occur. (Increasing α merely changes the scales of Fig. 2 because both α and C are scaled by $|\Delta w_0|$, and wavelength is scaled by $\Delta w_0^2/g$.) As with the zero-gravity jet case, these acoustic modes are attenuated until the pseudo-gas conditions are reached at very long wavelength.

The two other solutions to eq. (42) are comparable to the third mode in the zero-gravity jet case, which had zero wave speed and was completely attenuated. However, in the finite-gravity case, these modes are manifested as two slowly propagating waves with speeds of order ± 1 (i.e. in dimensional units at $\pm|\Delta w_0|$). These slow waves are simple porosity waves, which travel at approximately the separation velocity. The downward travelling slow waves are attenuated much as for the zero-gravity jet. However, the slow upward wave has a positive growth rate that increases rapidly with decreasing wavelength. This instability suggests that the basic-state uniform column is unstable and readjusts to a different structure; the large growth rate at vanishingly small wavelengths implies that the

readjustment involves formation of one or more sharp features, such as a shock (as shown in Section 5).

As with the simple zero-gravity jet case, at intermediate wavelengths, the acoustic waves vanish and only slow porosity waves exist. In this regime, sound waves are blocked and pressure changes can only be transmitted by slow porosity waves.

Overall, the extension to waves in a gravitationally segregating jet shows that acoustic waves propagate very similarly to the much simpler non-segregating (zero-gravity) jet; thus, much of the intuition gained in the simpler analysis holds. Although porosity waves propagate slowly, they can be unstable and control the adjustment of the uniform column to one with a sharp, shock structure, which is the subject of the next section.

5 NON-LINEAR STEADY-STATE ERUPTIONS

5.1 Governing equations

The development of shock structures and choking can be demonstrated by investigating the 1-D finite-amplitude variations in porosity, gas density and velocities in a steady-state erupting column.

We assume the mixture passes a level $z = 0$, presumably the fragmentation point, at which both phases are momentarily ascending at the same velocity $\mathcal{W}_0$. The initial gas density at this height is ρ_0 and the initial volume fraction is ϕ_0. In steady state, eqs (12) and (13) dictate that the fluxes $\rho_g \phi w_g$ and $(1 - \phi) w_m$ are determined by their values at $z = 0$ and do not change with increased height; that is

$$w_g = \frac{\rho_0 \phi_0 \mathcal{W}_0}{\rho_g \phi} = \frac{\phi_0 \mathcal{W}_0}{\theta \phi}, \tag{43a}$$

$$w_m = \frac{(1 - \phi_0)\mathcal{W}_0}{1 - \phi}, \tag{43b}$$

where again $\theta = \rho_g / \rho_0$. Using eq. (43) to eliminate the vertical velocities from the momentum eqs (14) and (15), and rescaling height to $z = (\mathcal{W}_0^2/g)z'$, we arrive at the dimensionless governing equations for ϕ and θ (where we drop the prime on z' after the necessary substitutions):

$$\frac{d}{dz}\left(\frac{\phi_0^2}{\theta \phi}\right) = -\bar{\alpha}^2 \phi \frac{d\theta}{dz} - \theta \phi + \Delta \mathcal{I}, \tag{44a}$$

$$\frac{d}{dz}\left(\frac{\beta_m (1 - \phi_0)^2}{1 - \phi}\right) = -\bar{\alpha}^2 (1 - \phi)\frac{d\theta}{dz} - \beta_m (1 - \phi) - \Delta \mathcal{I}, \tag{44b}$$

where the dimensionless vertical interaction force is

$$\Delta \mathcal{I} = \mathcal{D}\Delta \mathcal{U} + \frac{1}{2}\check{\beta}\check{\mathcal{U}}\frac{d\Delta \mathcal{U}}{dz} \tag{45}$$

in which

$$\Delta \mathcal{U} = \frac{1 - \phi_0}{1 - \phi} - \frac{\phi_0}{\theta \phi}, \tag{46}$$

$$\check{\mathcal{U}} = \frac{\beta_m \phi^2 (1 - \phi_0) + \phi_0 (1 - \phi)^2}{\phi(1 - \phi)\left(\beta_m \phi + \theta(1 - \phi)\right)}, \tag{47}$$

$\bar{\alpha} = \mathcal{C}_g / \mathcal{W}_0$ is the dimensionless sound speed (or its inverse is the mixture's Mach number), $\beta_m = \rho_m/\rho_0$, $\check{\beta} = \check{\rho}/\rho_0$ and $\mathcal{D} = \frac{c\mathcal{W}_0}{\rho_0 g}$.

Although $\bar{\alpha}$ and β_m are constant parameters, both $\check{\beta}$ and $\mathcal{D}$ are still functions of ϕ and θ. In particular, $\check{\beta} = \check{\rho}/\rho_0$, which is variable (see eq. A12). The dimensionless drag coefficient $\mathcal{D}$ is given by (using eq. A9 with eq. A8; Appendix A1)

$$\mathcal{D} = \mathcal{D}_0 (1 - \phi) + \mathcal{D}_\tau (1 - \phi)\theta|\Delta \mathcal{U},| \tag{48}$$

where

$$\mathcal{D}_0 = \frac{\bar{c}\mathcal{W}_0}{\rho_0 g} = \frac{\mu_g \mathcal{W}_0}{r^2 \rho_0 g} \tag{49}$$

is the dimensionless reference laminar drag coefficient on a particle of size r moving through the gas phase, and

$$\mathcal{D}_\tau = \frac{\mathcal{W}_0^2}{rg} \tag{50}$$

is the dimensionless turbulent drag coefficient for the same particle.

5.1.1 Dimensionless parameter ranges

The governing dimensionless parameters are $\beta_m, \bar{\alpha}, \mathcal{D}_0$ and $\mathcal{D}_\tau$. The density ratio β_m is assumed to be simply 100, because it is with respect to the gas density only at the fragmentation level, which is several tens of $kg\,m^{-3}$. The initial eruption velocity $\mathcal{W}_0$ is assumed to be between a few to several tens of $m\,s^{-1}$ and thus the dimensionless gas sound speed parameter is $10 \leq \bar{\alpha} \leq 100$. For a particle size range 10^{-4} m $\leq r \leq 10^{-2}$ m, and an initial velocity range $5\,m\,s^{-1} \leq \mathcal{W}_0 \leq 50\,m\,s^{-1}$, the drag coefficients go from $\mathcal{D}_0 = 10^{-3}$ and $\mathcal{D}_\tau = 250$ for the largest particles and smallest velocities, to $\mathcal{D}_0 = 10^2$ and $\mathcal{D}_\tau = 2.5 \times 10^6$ for smallest particles and largest velocities. In fact $\mathcal{D}_\tau \gg \mathcal{D}_0$, thus the size of $\mathcal{D}_0$ has little influence; we thus assume for simplicity that $\mathcal{D}_0 = 1$ and vary only the turbulent drag so long as $\mathcal{D}_\tau \gg 1$. For a summary of parameter values, see Table 2.

5.2 Simple limits

The non-linear steady-state equations admit a variety of solutions under certain important limits. In addition to the completely general system of a separating, compacting mixture with a compressible gas phase, we can also consider (1) the compacting two-phase system with incompressible gas, (2) the non-compacting (constant gas volume fraction ϕ) system with compressible gas and (3) the pseudo-gas system. The systems with compressible gas undergo singularities in gas density at finite height, which are associated with shock development and the choking condition.

5.2.1 Incompressible gas

The incompressible gas limit is useful for isolating the effects of compaction in the absence of gas expansion. This limit is obtained by setting the dimensionless gas density $\theta = 1$. The governing equation arises from the difference between $(1 - \phi)$ times (44a) and ϕ times (44b); this yields

$$\phi \frac{d}{dz}\left(\frac{\beta_m (1 - \phi_0)^2}{1 - \phi}\right) - (1 - \phi)\frac{d}{dz}\left(\frac{\phi_0^2}{\phi}\right)$$
$$= -\phi(1 - \phi)(\beta_m - 1) - \Delta \mathcal{I}, \tag{51}$$

which is an ordinary differential equation for ϕ. Because the gas is incompressible, there is no dependence on $\bar{\alpha}$ (i.e. sound speed). This system displays no singularities associated with shock development and choking, and in fact approaches a flat profile in ϕ as

the forces associated with gravitational segregation and inter-phase drag balance. For example, assuming $\beta_m \gg 1$ and $\mathcal{D}_\tau \gg \mathcal{D}_0$, (51) reduces (after some algebra) to a simplified form

$$\frac{d\phi}{dz} = -\frac{\beta_m \phi^3(1-\phi)^3 - \mathcal{D}_\tau(1-\phi)(\phi-\phi_0)^2}{\beta_m \phi^3(1-\phi_0)^2}. \tag{52}$$

The gas volume fraction flattens ($d\phi/dz = 0$) at a finite ϕ given by the relation

$$\frac{(\phi-\phi_0)^2}{\phi^3(1-\phi)^2} = \frac{\beta_m}{\mathcal{D}_\tau}, \tag{53}$$

which indicates the minimum ϕ reached after compaction, for a given ratio $\beta_m/\mathcal{D}_\tau$. For moderate drag in which $\beta_m/\mathcal{D}_\tau \approx 1$, compaction will, for example, drive porosity from $\phi = \phi_0 = 0.7$ to $\phi_f \approx 0.5$, where ϕ_f is the solution to eq. (53); for large drag in which $\beta_m/\mathcal{D}_\tau \approx 10^{-2}$, the porosity collapses only to $\phi \approx 0.68$ (Figs 3 and 4). The compaction height can be crudely approximated by $h = (\phi_f - \phi_0)/[d\phi/dz]_{\phi_0} \approx \phi_0 - \phi_f$. Therefore, compaction is both diminished and completed within a shorter distance as turbulent drag increases.

5.2.2 Fixed gas volume fraction

The fixed gas volume fraction (i.e. fixed ϕ) limit is useful for examining the effects of gas expansion in the absence of mixture compaction. Physically, however, this case is more relevant for gas flowing through a rigid or slowly deforming porous medium, as might occur in highly vesiculated magmas with interconnected pore space (Gonnermann & Manga 2007). The governing equation is obtained by setting $\phi = \phi_0$ and summing eqs (44a) and (44b) to eventually yield

$$\frac{d\theta}{dz} = -\frac{\theta^2[\beta_m(1-\phi_0)+\phi_0\theta]}{\bar{\alpha}^2\theta^2 - \phi_0}. \tag{54}$$

The implicit analytic solution for the gas density θ from this equation (given the boundary condition that $\theta = 1$ at $z = 0$) is

$$z = \frac{\phi_0}{\beta_m(1-\phi_0)}\left(1 - \frac{1}{\theta}\right)$$

$$+ \log\left(\theta^{\frac{-\phi_0^2}{\beta_m^2(1-\phi_0)^2}}\left[\frac{\beta_m(1-\phi_0)+\phi_0\theta}{\beta_m(1-\phi_0)+\phi_0}\right]^{\frac{\phi_0^2}{\beta_m^2(1-\phi_0)^2} - \frac{\bar{\alpha}^2}{\phi_0}}\right). \tag{55}$$

Because both $\bar{\alpha}^2$ and β_m are typically $\gg 1$, the solution (55) is close to the straight line approximation

$$\theta = 1 - \frac{\beta_m(1-\phi_0)}{\bar{\alpha}^2}z \tag{56}$$

for much of the domain over which the solution exists. However, this domain ends where eq. (54) is singular, which occurs at $\theta = \theta_c \equiv \sqrt{\phi_0}/\bar{\alpha}$. This singularity constitutes a shock and the choking condition since $\frac{d\theta}{dz} \to \infty$ at this point. The gas velocity at the choking point is given by eq. (43), which yields (with $\phi = \phi_0$)

$$w_g = \frac{\mathcal{W}_0}{\theta_c} = \frac{\bar{\alpha}\mathcal{W}_0}{\sqrt{\phi_0}} = \frac{\mathcal{C}_g}{\sqrt{\phi_0}}. \tag{57}$$

Given that $\phi_0 \sim O(1)$, the gas velocity at the choking point is slightly in excess of the gas sound speed, which is due to the rigid porous matrix impeding gas expansion, thereby imparting an additional effective incompressibility to the gas.

5.2.3 Pseudo-gas

The pseudo-gas approximation assumes that the magma particle and gas phases are locked together and thus have the same velocity (Section 4.1.1). This limit is useful for illustrating the effect of gas expansion on gas volume fraction ϕ, but in the absence of compaction due to phase separation. Setting $w_g = w_m$ from eq. (43) one obtains in this case

$$\phi = \frac{\phi_0}{\theta(1-\phi_0)+\phi_0} \tag{58}$$

and that $w_g = w_m = \phi_0/(\theta\phi)$. The pseudo-gas momentum equation is given by the sum of eqs (44a) and (44b), which, with the substitution of ϕ from (58), eventually leads to

$$\frac{d\theta}{dz} = -\frac{\theta^3[\beta_m(1-\phi_0)+\phi_0]}{[\theta(1-\phi_0)+\phi_0][\bar{\alpha}^2\theta^2 - \phi_0(\beta_m(1-\phi_0)+\phi_0)]}. \tag{59}$$

The implicit analytic solution for the gas density θ from this equation (given the boundary condition that $\theta = 1$ at $z = 0$) is

$$z = \frac{\bar{\alpha}^2[(1-\phi_0)(1-\theta)-\phi_0\log\theta]}{\phi_0 + \beta_m(1-\phi_0)} - \frac{\phi_0(1-\theta)[\phi_0(1-\theta)+2\theta]}{2\theta^2}. \tag{60}$$

However, eq. (59) is singular at

$$\theta = \theta_c \equiv \frac{1}{\bar{\alpha}}\sqrt{\phi_0(\beta_m(1-\phi_0)+\phi_0)} = \mathcal{W}_0/\mathcal{C}_\psi, \tag{61}$$

where $\mathcal{C}_\psi$ is the reduced pseudo-gas sound speed given by eq. (27) (Section 4.1.1). (Vergniolle & Jaupart (1986) arrived at similar conditions although they did not account for variations in gas mass fraction in the column.) As with the fixed ϕ case, the erupting column develops a shock, which is associated with a choking condition. The velocity at this choking point (in either phase) is

$$w_g = w_m = (1-\phi_0)\mathcal{W}_0 + \phi_0\mathcal{C}_\psi, \tag{62}$$

which is slightly less than the reduced sound speed $\mathcal{C}_\psi$ (assuming $\mathcal{W}_0 < \mathcal{C}_\psi$), and considerably less than the gas velocity in the fixed ϕ case at the choking point. We will see that the full two-phase system, with compaction, phase separation and gas compression, still leads to choking, but with more plausible eruption velocities at the choking point than the simple pseudo-gas limit suggests.

5.3 General two-phase system

5.3.1 Choking conditions

As noted already, the development of a shock in a steady erupting column occurs when the gas density becomes discontinuous, that is as $\frac{d\theta}{dz} \to \infty$; we can determine the conditions for this shock in the general system by examining eq. (44) in this limit. Considering both the sum of (44a) and (44b), as well as (44b) by itself, and retaining only terms that are multiplied by $\frac{d\theta}{dz}$ (assuming that $\frac{d\phi}{dz}$ is non-singular), we arrive at

$$\bar{\alpha}^2\theta^2 - \phi_0^2/\phi = 0 \tag{63}$$

and

$$-\bar{\alpha}^2(1-\phi) + \frac{1}{2}\breve{\beta}\breve{\mathcal{U}}\frac{\partial\Delta\mathcal{U}}{\partial\theta} = 0. \tag{64}$$

Assuming $\beta_m \gg 1$ leads to $\breve{\beta}\breve{\mathcal{U}}\partial\Delta\mathcal{U}/\partial\theta = \phi_0(1-\phi_0)/(\phi\theta)$ and hence eq. (64) leads to

$$\theta = \frac{1}{2}\frac{\phi_0(1-\phi_0)}{\bar{\alpha}^2(1-\phi)}. \tag{65}$$
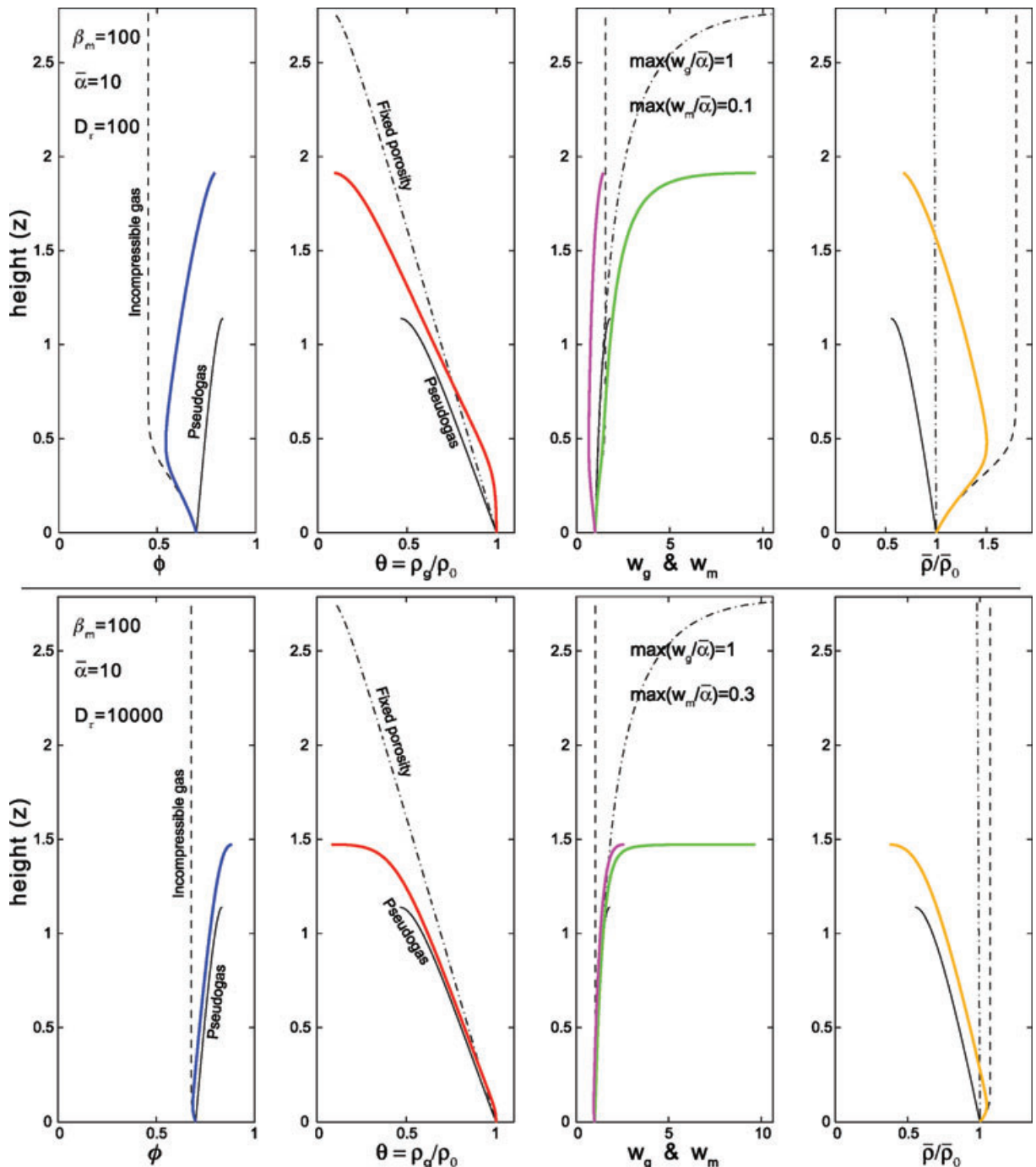
**Figure 3.** Porosity ϕ, dimensionless gas density θ, gas and magma velocities w_{g} (green) and w_{m} (magenta), and mixture density $\bar{\rho}$ normalized by the value at $z = 0$. Cases shown are for a high input velocity $\mathcal{W}_0$ such that $\bar{\alpha} = \mathcal{C}_{\mathrm{g}}/\mathcal{W}_0$, and two different dimensionless turbulent drag coefficients numbers $\mathcal{D}_\tau$, as indicated, top and bottom panels. (The laminar drag coefficient $\mathcal{D}_0$ is set to 1 for all cases, since $\mathcal{D}_\tau \gg \mathcal{D}_0$.) Key parameters are indicated on the left frames. Dashed curves indicate the solution with incompressible gas in which dimensionless density is fixed to $\theta = 1$ (eq. 51); the dash-dot curves indicate the solution for gas volume fraction fixed to $\phi = \phi_0$ (eq. 55); and the thin black curves are solutions for the pseudo-gas model (eq. 60). For the velocity plot, only the gas velocity is shown for the incompressible and fixed-porosity models, whereas the pseudo-gas model implicitly has only one velocity.

Eliminating ϕ between (63) and (65) leads to the choking condition

$$\theta_c = \frac{1}{4\bar{\alpha}^2}\left(\phi_0(1 - \phi_0) + \sqrt{\phi_0^2(1 - \phi_0)^2 + 16\phi_0^2\bar{\alpha}^2}\right), \qquad (66)$$

which, given that generally $\bar{\alpha} \gg 1$, can be approximated by $\theta_c = \phi_0/\bar{\alpha}$. Thus, the gas density at the choking point in the general two-phase system is less than that predicted by the pseudo-gas by

a factor of approximately $\sqrt{\beta_{\mathrm{m}}(1 - \phi_0)/\phi_0 + 1}$ (see eq. 61); this means that for a typical $\beta_{\mathrm{m}} = 100$ and $\phi_0 = 0.7$, the gas density at choking for a pseudo-gas is about seven times larger than that for the general two-phase case. The two-phase choking condition is also associated with a gas volume fraction of $\phi \approx 1$ (inferred from 63) and a gas velocity reaching $w_{\mathrm{g}} = \mathcal{W}_0\phi_0/(\theta\phi) \approx \mathcal{W}_0\bar{\alpha} = \mathcal{C}_{\mathrm{g}}$ (from eq. 43). (Kozono & Koyaguchi (2009a) arrive at a similar condition
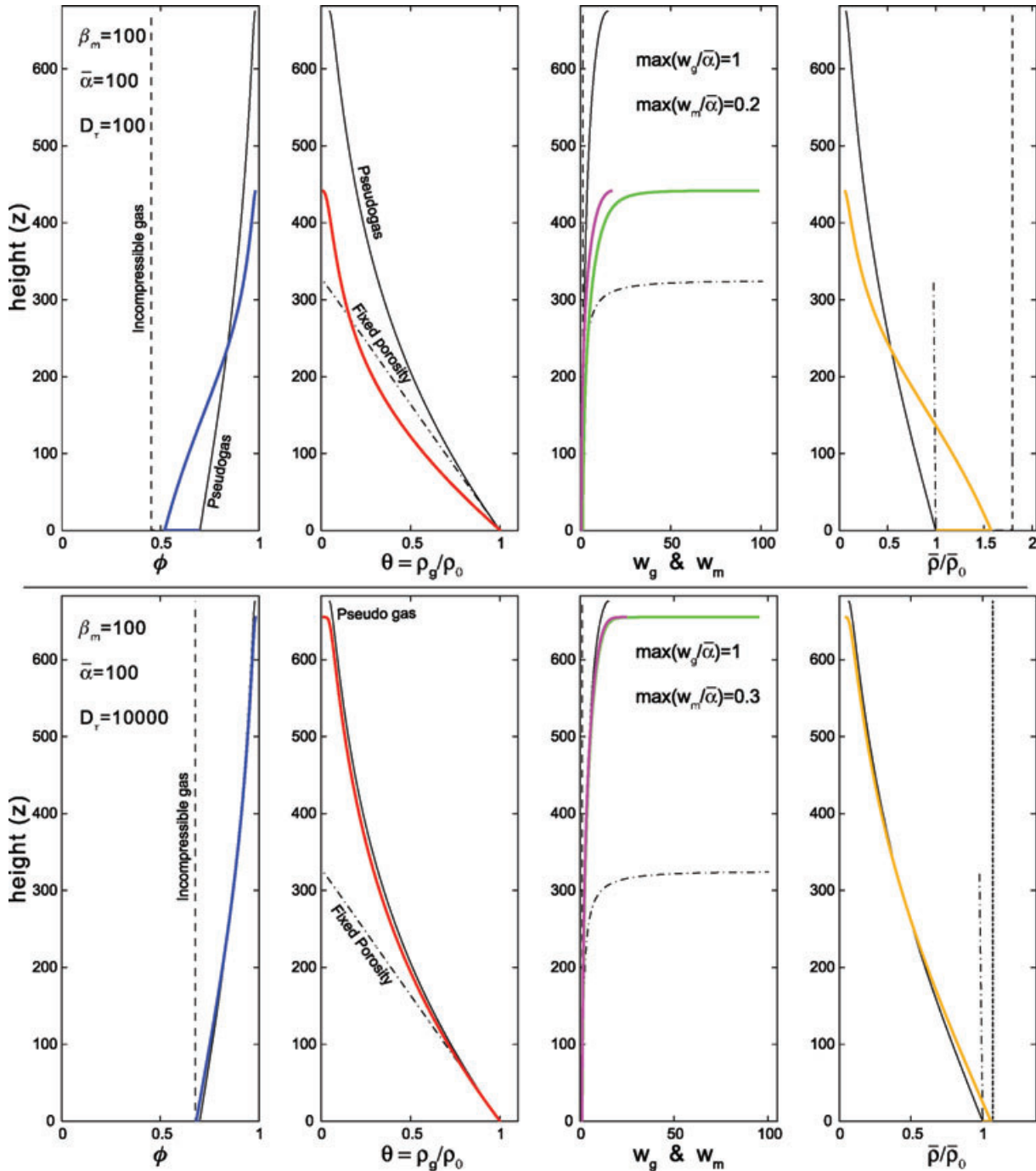
Figure 4. Same as Fig. 3, except a low input velocity $\mathcal{W}_0$ such that $\bar{\alpha} = \mathcal{C}_g/\mathcal{W}_0 = 100$.

in the same limit of $\phi \to 1$.) This approximate analysis is only valid in the limit $\bar{\alpha} \gg 1$ and in fact poorly predicts particle velocity $\mathcal{W}_0(1 - \phi_0)/(1 - \phi)$, which depends entirely on the inaccuracy of the approximation for ϕ (i.e. how much ϕ deviates from 1).

5.3.2 Numerical solutions

The governing equations for 1-D steady-state eruptions are given by eq. (44), the mathematical solutions of which are discussed in more detail in Appendix C2. The solutions are integrated numerically by standard schemes (e.g. adaptive-step Runge–Kutta method) for initial value problems for coupled non-linear ordinary differential

equations. For comparison, we also solve the system of equations in three other limits: (a) the incompressible gas case (by numerical integration of eq. 51); (b) the fixed gas volume fraction case (from eq. 55) and (c) the pseudo-gas case (from eq. 60).

Numerical solutions display a variety of behaviour depending on the initial velocity (or, alternatively, gas compressibility) and turbulent drag (Figs 3 and 4). In essence, there are three competing effects: compaction due to gravitational deceleration of particles, gas decompression during ascent and turbulent drag coupling the gas and particles.

Effect of eruption velocity on simple cases. Before considering the effects of compaction and phase separation, we examine the

dramatic disparity in behaviour between the two simple limits for which compaction is precluded, that is the fixed-ϕ and pseudo-gas cases. The difference in behaviour is most notable in the gas density (i.e. compare profiles in θ for Figs 3 and 4). For lower $\bar{\alpha}$ (large initial velocity), gas expands more rapidly for the pseudo-gas case than the fixed-ϕ case, whereas the opposite occurs for larger $\bar{\alpha}$ (smaller initial velocity). The cause for this switch in behaviour is instructive for understanding the results of the general two-phase model.

For small velocity (large $\bar{\alpha}$; Fig. 4), especially with $\bar{\alpha}^2 \gg \beta_m \gg 1$, the dynamic pressure of either phase (i.e. $\rho_j w_j^2$, where $j = g$ or m) is small relative to the gas pressure ($\mathcal{C}_g^2 \rho_g \propto \bar{\alpha}^2 \theta$). The gas pressure gradient is thus nearly hydrostatic and determined by the weight of the mixture, which is dominated by the magma component's weight, which goes approximately as $\beta_m(1 - \phi)$; this weight is nearly constant for the fixed-ϕ case, but decreases for the pseudo-gas case as the gas expands and ϕ increases. (In particular, note that in the limit $\bar{\alpha}^2 \gg \beta_m \gg 1$, eq. (54) for the fixed-ϕ case gives a pressure gradient $\bar{\alpha}^2 \frac{d\theta}{dz} \approx -\beta_m(1 - \phi_0)$, whereas eq. (59) for the pseudo-gas gives $\bar{\alpha}^2 \frac{d\theta}{dz} \approx -\frac{\beta_m(1-\phi_0)\theta}{\theta(1-\phi_0)+\phi_0}$.) Thus, the pressure and gas density gradients start off nearly identically at $z = 0$ but the pseudo-gas pressure gradient decreases in magnitude with increasing height.

For larger velocity (smaller $\bar{\alpha}$; Fig. 3), especially with $\bar{\alpha}^2$ of the same order as β_m, the dynamic pressure can become important. However, for the fixed-ϕ case, the particle velocity is fixed (eq. 43) and thus there is no change in the particle dynamic pressure, whereas the gas dynamic pressure is always small; thus, the pressure gradient does little work to change dynamic pressure and the system remains close to hydrostatic (eq. 56). For the pseudo-gas model, the particle dynamic pressure is large and increases with height (i.e. as gas expands the mixture velocity increases) and thus the gas pressure drops accordingly (e.g. as predicted by Bernoulli's principle), causing a steeper pressure and gas density gradient.

Effects of eruption velocity on the general two-phase system. In the absence of other effects, the particle ascent against gravity slows down within a dimensionless height of $z \approx \frac{1}{2}$, which is dimensionally $\frac{1}{2}\mathcal{W}_0^2/g$, that is the height over which the initial particle kinetic energy is lost to increased gravitational potential energy. As the particles slow down the mixture compacts. The effect of compaction on gas density depends on how much gas decompression would have occurred over this length scale naturally, because compaction acts to impede expansion. Moreover, because the compaction height depends on deceleration of the particles, the gas drag plays an important role in that it imparts momentum to the particles and curtails deceleration (e.g. see discussion of the incompressible-gas system; Section 5.2.1).

Fast initial eruption. For relatively high initial velocities (i.e. smaller ratio of gas sound speed to initial flow speed, e.g. with $\bar{\alpha} \approx 10$, Fig. 3), the gravitational deceleration of particles and hence compaction of the mixture occurs over a height comparable to the scale height for gas decompression, thereby causing decompression to be inhibited by compaction. In particular, although compaction due to gravitational deceleration of particles occurs over a dimensionless height of approximately $\frac{1}{2}$ (for low to moderate turbulent drag), the free gas decompression (which, without compaction, is well approximated by eq. 56) occurs over a dimensionless scale height of $\frac{\bar{\alpha}^2}{\beta_m(1-\phi_0)}$; this height is of order unity for $\bar{\alpha} \approx 10$ and $\beta_m \approx 100$ (in fact, for this case, with $\phi_0 = 0.7$ the free decompression height is $(1 - \phi_0)^{-1} \approx 3$ as shown in Fig. 3). Dimensionally, the compaction height is $\frac{1}{2}\mathcal{W}_0^2/g$, whereas the free decompression scale height is $\mathcal{C}_g^2/(\beta_m g(1 - \phi_0))$, which become comparable for

large enough initial velocity $\mathcal{W}_0$. The interaction of compaction and decompression thus causes the following effects if initial velocity is high and turbulent drag is moderate (Fig. 3, top panel):

(1) During ascent, the gas volume fraction ϕ collapses initially (following a trajectory close to that for the incompressible gas model) before increasing gradually during gas expansion, an effect not captured by the pseudo-gas model, which predicts only steady increase of porosity under gas expansion.

(2) Decompression of gas is impeded and gas density remains almost constant during initial compaction. After the particles have lost their initial kinetic energy and the gravitational compaction peaks, gas expansion increases more rapidly and drives decompaction (dilation) of the mixture. Because of the increase in the magma component's dynamic pressure with height, the gas pressure and density drops more rapidly than in the fixed-ϕ model. Gas density also drops slightly more rapidly than in the pseudo-gas case because, with moderate turbulent drag, the gas can separate and escape the mixture, thus permitting less constrained expansion. Even so, the pseudo-gas model predicts gas density to drop steadily from the initial value and thus underpredicts gas density at a given height. The pseudo-gas choking point occurs lower in the column because it is reached when the gas density is still at a fairly large value, whereas the general-model choking point occurs higher after reaching a much lower gas density; the hypothetical fixed-ϕ choking point occurs at an even greater height for this case due to the shallower nearly hydrostatic pressure gradient.

(3) During compaction and deceleration of the magma component, the particles lag the gas over the height of the column and thus have significantly lower velocities than the gas even at the choking point. The pseudo-gas model generally over-estimates magma particle velocities, and predicts they will be comparable to the gas velocity. The choking point for the pseudo-gas is achieved when this over-estimated mixture velocity is comparable to the reduced mixture sound speed. Choking conditions for both the general two-phase and the fixed-ϕ model occur when the gas velocity reaches the gas sound speed, which in this case happens higher in the column. The incompressible gas model has very little variation in either phase's velocities, which demonstrates that the rapid acceleration toward the choking point in the other models is entirely driven by gas expansion.

(4) Finally, the mean mixture density increases significantly during the compaction phase—initially along a trajectory close to that for the incompressible-gas model—and then decreases steadily thereafter. The pseudo-gas model predicts the mixture density to decrease always and thus significantly under-predicts mean density at a given height. (The fixed-ϕ model predicts essentially no change in mean mixture density because, even with change in gas density, the mean density is dominated by the magma component, proportional to $\beta_m(1 - \phi_0)$, which remains constant.)

The general two-phase and pseudo-gas models have different predictions of mixture density and particle velocity at given depths, but they reach comparable values at the choking point, although this is predicted to occur at very different depths in these models. However, the differences between the general two-phase model and the pseudo-gas model are accentuated for lower turbulent drag coefficient $\mathcal{D}_\tau$. For larger drag (Fig. 3, bottom panel), the initial compaction height is smaller than the gravitational deceleration height of (non-dimensionally) $\frac{1}{2}$. In this case, the increased drag causes the phases to dynamically equilibrate more rapidly (i.e. approach the same velocity), and thus the particles do not fully decelerate under

gravity before being entrained and accelerated by the gas during its expansion. Other than the shorter initial compaction length, the results and interpretations remain qualitatively the same. However, it is notable that with increased drag the general model approaches the pseudo-gas case, and the two phase's velocities are more comparable over much of the column, as is to be expected, except near the choking point. More striking yet is that with increased turbulent drag, choking is more abrupt and dramatic and occurs lower in the column than with moderate drag; this occurs because drag accelerates the magma component and increases its dynamic pressure, which is compensated by a rapid drop in gas pressure and density.

Slower eruptions. For smaller initial velocities (larger $\bar{\alpha}$; Fig. 4), the gravitational deceleration and compaction height is much smaller than the gas decompression scale height. Thus, the initial collapse of the gas volume occurs within a very short distance over which porosity drops and mean mixture density increases abruptly (Fig. 4, top panel), but gas density changes very little. The magnitude of these abrupt changes depends on the turbulent drag which mitigates the particle deceleration and resultant compaction (Fig. 4, bottom panel).

After initial compaction, the dynamics of the column is dominated by gas decompression. As noted earlier, in the simple fixed-ϕ and pseudo-gas limits, the changes in gas density are dictated by nearly hydrostatic pressure gradients; because the fixed-ϕ case has a nearly constant mixture weight the pressure gradient is constant over much of the column, whereas for the pseudo-gas case the mixture weight decreases as the gas expands and ϕ increases. In the general two-phase model, compaction initially collapses the gas volume near the base of the column; the mixture therefore ascends with an initially smaller ϕ and a larger initial average density and weight (see Fig. 4, top panel, ϕ and $\overline{\rho}$ profiles), and hence steeper pressure and gas density gradients than either of the two simpler models (Fig. 4 top panel, θ profile). However, as gas expands the mixture density and weight drop rapidly and the pressure gradient flattens up until the final shock and choking point. The choking point for the slower velocity cases occurs lower (instead of higher) than in the pseudo-gas model because the pseudo-gas maintains a more gradual hydrostatic pressure gradient. (The pseudo-gas also reaches choking at a much smaller gas density than it does when velocity is larger ($\bar{\alpha}$ is smaller); see eq. 61).

The phase's velocities are also mostly dictated by gas expansion and coupling between phases. With initial gravitational deceleration having been achieved low in the column, the magma particles are mostly entrained by the gas through turbulent drag and have comparable velocities up to the choking point. The choking point occurs when the gas separates from the mixture and rapidly reaches the gas sound speed.

With increased drag and smaller velocities (Fig. 4, bottom panel), the general two-phase model is closer to the pseudo-gas than in any other scenario. Compaction only affects the column if the abrupt collapse of the gas volume near the base effectively resets the starting porosity and mean density, and hence pressure gradients, near $z = 0$. But with increased drag, this initial collapse itself is nearly eliminated and thus the general and pseudo-gas models begin ascent nearly identically, and with high turbulent drag remain nearly identical; their only significant difference is in where they reach the choking point because at high enough porosity the turbulent drag becomes small enough for the gas to rapidly separate from the mixture and reach sound speed, whereas the pseudo-gas phases never separate.

6 DISCUSSION

The full two-phase treatment of volcanic conduit eruptions displays diverse behaviour and significant differences with classical simplifications such as the pseudo-gas model. In this study, we have primarily focussed on the effect of two-phase interactions on acoustic wave propagation, and the interaction of compaction, phase separation and compression on shock development and choking.

6.1 Acoustic-porosity waves and shock development

The analysis of combined acoustic and porosity waves (for both the non-separating zero-gravity and the gravitationally segregating erupting columns) show that sound waves are highly dispersive in which small-wavelength waves travel much faster than long-wavelength waves, while intermediate wavelengths are blocked entirely. Long-wavelength waves are associated with stronger phase coupling because the inertial lag between phases is less at low frequencies, and thus drag is more effective; in this limit, the wave speed approaches the pseudo-gas sound speed. Attenuation is generally largest at shortest wavelengths and approaches zero as the phase locking becomes perfect (i.e. the perfect pseudo-gas waves are undamped).

The inferred wave dispersion implies that short-wavelength disturbances on an erupting column will only induce shocks if the column's gas velocity reaches the gas sound speed. Long-wavelength disturbances will start to develop shocks if the column is erupting at least as fast as the reduced pseudo-gas sound speed. (Intermediate wavelength disturbances that coincide with sound blocking will induce shocks at any column velocity.) However, steepening by shock development will force the long-wavelength disturbances toward shorter wavelengths, at which point they can conceivably propagate up to the pure gas sound speed without inducing shocks. This dispersive behaviour provides a natural mechanism by which long wavelength disturbances begin to choke and then unchoke by shock steepening. However, this implies that, in the end and regardless of wavelength, the only real condition for shock development and choking is when the eruption velocity of the gas reaches the gas sound speed.

Most of the wave-like perturbations (acoustic and porosity waves) are attenuated and thus the column is generally stable to such perturbations. However, in the gravitationally segregating column, one slow-moving porosity wave has positive growth rate, which increases at shorter wavelength (Fig. 2). This instability implies that the zeroth-order uniform column is not stable and undergoes readjustment. However, the column necessarily readjusts to the final steady-state column displayed in the non-linear analysis (Figs 3 and 4), and the small wavelength instability is indicative of shock development during this readjustment. Moreover, because the shock is a small wavelength structure it propagates at the maximum wave speed, that is the acoustic velocity of the gas, and not at some reduced sound speed.

6.2 Interaction of compaction, compression and turbulent drag in the erupting column

The finite–amplitude interaction of compaction, compression, interphase turbulent drag and their effect on shock development are illustrated by the non-linear steady-state calculations (Section 5). Compaction of the mixture is largely determined by the initial gravitational deceleration of the particles, which, in the absence of other

effects occurs within a length scale of $\frac{1}{2}\mathcal{W}_0^2/g$, where $\mathcal{W}_0$ is the initial vertical velocity. For relatively fast initial eruption velocities (approximately an order of magnitude slower than sound speed), the mixture compaction and gas decompression lengths are comparable, and thus compaction impedes gas expansion, keeping gas density nearly constant over the compaction length. Once compaction ceases and gas expansion dominates, the large increase in dynamic pressure for the fast-moving mixture causes a relatively steep drop in pressure and hence gas density (i.e. steeper than in the hydrostatic state).

With slower eruption velocity (e.g. approximately 100 times slower than gas speed), the compaction length is very short and compactive adjustment of the gas volume fraction happens rapidly near the base of the column (following fragmentation). Simple gas expansion dominates over the rest of the column, and is only affected by compaction in so far as the initial gas volume fraction and hence mean density has been reset near the column base. Moreover, with a slower mixture velocity the dynamic pressure effects are small and thus the gas pressure and density gradients are primarily hydrostatic and more gradual.

The effect of turbulent inter-phase drag is to reduce gravitational deceleration of particles during compaction and to shorten the compactive length scale. The drag can be related to particle size, and in particular erupting flows with large particles are more affected by compaction as they have a smaller turbulent drag coefficient $\mathcal{D}_\tau$. In contrast, flows with small particles have magma velocities close to the gas velocity (Figs 3 and 4, compare top frames to bottom ones). For flows with large drag (small particles) the system approaches the pseudo-gas state as expected (except near choking), although this is more pronounced for slower-velocity eruptions (Fig. 4). Flows with larger post-fragmentation velocities have the largest deviation from a pseudo-gas because of the increased effect of simultaneous compaction and compression.

6.3 Choking

As predicted by the choking conditions, the non-linear steady-state erupting columns develop a discontinuity, or shock, in gas density and velocity, hence undergo choking (except in the case of incompressible gas). The dimensional height at which choking occurs has relatively little variation, even over large ranges in initial velocity and turbulent drag. The non-dimensionalizing length scale for Figs 3 and 4 is $\mathcal{W}_0^2/g$; thus, assuming gas sound speed is fixed, the figure with $\bar{\alpha} = \mathcal{C}_g/\mathcal{W}_0 = 10$ has a dimensional scale 100 times larger than the $\bar{\alpha} = 100$ case. For larger initial velocities of order $50\ \text{m s}^{-1}$ ($\bar{\alpha} = 10$, Fig. 3), choking occurs within a height of $H_c \sim 2\mathcal{W}_0^2/g$, which is of order several hundreds of metres after fragmentation. For slower velocities of order $5\ \text{m s}^{-1}$ ($\bar{\alpha} = 100$, Fig. 4), choking occurs at a height of $H_c \sim 500\mathcal{W}_0^2/g$, which is slightly higher and of order 1 km. Thus, choking conditions are reached earlier for high initial velocity than for low initial velocity, but only by a factor of 2–3 for a factor of 10 difference in velocity.

Choking in the general system occurs at a different height than that predicted by the pseudo-gas model, but the difference is dependent on post-fragmentation velocity. For high initial velocity, choking occurs slightly higher in the column (above the fragmentation point) for the general system than for a pseudo gas, whereas the reverse is true for lower velocity. This disparity occurs because, at high velocities, choking in the pseudo-gas occurs at a relatively large gas density and is thus more easily reached; moreover, compaction inhibits gas decompression in the general system, and thus

delays shock development. For slow velocity, compaction has little effect on gas density but collapses the gas volume fraction abruptly near the column base, leading to a larger initial mixture density and weight, hence sharper gradients and more rapid drop in gas pressure for the general system.

Increased turbulent drag, or reduced particle size, causes the location of the shock to approach that of the pseudo-gas. However, increased drag also sharpens the shock structure remarkably; this occurs because as drag increases the particle velocity, the dynamic pressure in the magma phase increases as well, which then causes a rapid drop in gas pressure and density.

Our analysis shows that choking conditions occur primarily in the gas phase, in particular when it reaches the gas sound speed $\mathcal{C}_g$, rather than when the entire medium reaches the reduced mixture sound speed. The pseudo-gas model therefore underpredicts the shock strength and velocity, because the shock propagates faster than the particles, in agreement with Chojnicki *et al.* (2006). At the choking point, the particle speed is always lower than that of the gas, depending on the value of the drag coefficient $\mathcal{D}_\tau$. At the choking point, the particle velocity is $\sim$5–10 times lower than the gas velocity for intermediate drag, and $\sim$2–3 times lower than the gas sound speed for large drag (i.e. small particle size), which is closer to the sound speed in the mixture.

Gas sound speed $\mathcal{C}_g$ is approximately $700\ \text{m s}^{-1}$ for water vapour at 1000–1300 K. Hence our results imply that observed eruption velocities of approximately $600\ \text{m s}^{-1}$ can be readily explained without invoking the special conduit nozzle geometries needed to induce 'supersonic' eruption speeds (i.e. supersonic relative to the pseudo-gas sound speed and choking velocity of about $150\ \text{m s}^{-1}$).

6.4 Eruptive pressure drop and secondary fragmentation

In all cases the gas density and pressure at the choking point are always smaller in the general two-phase system than in the pseudo-gas model. The difference in pressure depends on the gas volume fraction and gas density at fragmentation (Section 5.3.2) but is typically about seven times smaller for the general two-phase flow. The pressures at the choking point and exit are not only important for estimating the starting conditions for vulcanian and plinian eruptions, but also for inferring effects associated with choking, such as secondary fragmentation.

The pressure at the choking point P_c can be deduced from the pressure P_0, gas volume fraction ϕ_0, and velocity $\mathcal{W}_0$ at fragmentation via eq. (66), which in the limit of $\bar{\alpha} \gg 1$ leads to $P_c = P_0\phi_0\mathcal{W}_0/\mathcal{C}_g$. Using conservative values of $P_0 = 25\ \text{MPa}$ (Section 3.2), $\phi_0 = 0.7$, $\mathcal{W}_0 \approx 5$–$50\ \text{m s}^{-1}$ and $\mathcal{C}_g \approx 700\ \text{m s}^{-1}$, we calculate a choking gas pressure of $P_c \approx 0.1$–$1\ \text{MPa}$. Thus, while both slow and fast initial eruptions pass through the choking point with the same gas velocity of approximately $\mathcal{C}_g$, they have very different gas pressures (and hence densities) which of course then continue to drive the eruptions to different altitudes.

The pressure drop can also induce secondary fragmentation, especially in larger particles. In particular, the rapid change in gas density and pressure during choking induces a large pressure drop across the interior of larger particles that have retained gas bubbles of higher density and pressure (obtained from the first fragmentation point at the base of the erupting column). A pressure drop of approximately 25 MPa is equivalent to or in excess of the tensile strength of even reasonably cohesive minerals (Lockner 1995, Fig. 10). In essence, the pressure drop would cause these larger

particles to explode. Moreover, because of their reduced drag, larger particles are more likely to lag the gas especially during the secondary eruption associated with choking and the sudden expansion and release of gas. The turbulent stresses (which go as $\mathcal{D}_\tau \Delta w^2$) on large particles peak at the choking point when the separation velocity Δw is greatest.

Both excess interior bubble pressures and turbulent stresses associated with choking might therefore lead to secondary fragmentation of preferentially large particles, as suggested by the size distribution of pyroclasts in explosive eruptions (Kaminski & Jaupart 1998).

7 SUMMARY AND CONCLUSION

We have presented a general two phase theory of high-velocity volcanic eruptions that includes gas compressibility, interphase turbulent drag and inertial interface momentum exchange. The theory is used to analyse acoustic porosity waves in an erupting column, and conditions for shock development and choking.

Acoustic waves in the general two-phase theory are highly dispersive in which waves propagate at the normal gas sound speed at short wavelengths, at the reduced mixture or pseudo-gas sound speed at large wavelengths, and are completely attenuated and blocked at intermediate wavelengths. Slow porosity waves propagate simultaneously with the sound waves. All waves are attenuated except the slow upward-propagating porosity wave; this latter wave is most unstable at shortest wavelengths, indicative that the uniform eruptive column along which the waves travel will structurally readjust to a sharper structure, in particular a shock.

Analysis of the non-linear, steady-state system shows that compaction has important effects on the eruptive column depending on initial eruptive velocity and turbulent drag (or particle size). Gas decompression is delayed by compaction especially in mixtures with large initial velocity. At lower velocities, compaction collapses the gas volume fraction at the base of the column, which then resets the mixture weight and increases the gradients in gas pressure and density. However, changes in dynamic pressure strongly influences the gas pressure and density profiles, especially in faster eruptions. Enhanced turbulent drag forces the system to behave more like a pseudo-gas, as expected, but also sharpens the shock front significantly.

Any eruptive conduit model with gas decompression develops a shock and reaches a choking condition. At this point, decompression happens rapidly, driving decompaction and a rapid eruption. The traditional pseudo-gas model predicts that choking occurs when the mixture velocity approaches the reduced pseudo-gas sound speed. The general two-phase theory predicts that choking occurs only when the gas phase approaches normal gas sound speed, in agreement with the experiments of Chojnicki *et al.* (2006) (see also Vergniolle & Jaupart 1986; Kozono & Koyaguchi 2009a). The exit or choking point gas velocity in eruptions has been estimated to be as high as 600 m s^{-1} (Wilson 1976; Wilson *et al.* 1980), and this disparity with choking and hence the implied velocity bounds at the slow pseudo-gas sound speed creates a 'slow choking' paradox. This paradox is typically circumvented by allowing variations in the conduit radius (e.g. Wilson *et al.* 1980; Mitchell 2005) in which pinching nozzle geometries (as in the de Laval converging-diverging jet nozzle) permit 'supersonic' velocities, that is relative to the slow pseudo-gas sound speed. However, such eruption velocities are exactly comparable to the pure gas sound speed, at which choking is predicted to occur in the general two-phase theory. Therefore, no special appeal to conduit geometry is necessary and the eruptive velocities are in keeping with the general two-phase physics of volcanic eruptions.

REFERENCES

Basset, A., 1961, *Treatise on Hydrodynamics*,Vol. 2, Deighton, Bell and Co., Cambridge (original publication 1888).

Bercovici, D. & Ricard, Y., 2003. Energetics of a two-phase model of lithospheric damage, shear localization and plate-boundary formation, *Geophys. J. Int.,* **152,** 581–596.

Bercovici, D. & Ricard, Y., 2005. Tectonic plate generation and two-phase damage: void growth versus grainsize reduction, *J. geophys. Res.,* **110,** B03,401, doi:10.1029/2004JB003181.

Bercovici, D., Ricard, Y. & Schubert, G., 2001a. A two-phase model of compaction and damage. 1. General theory, *J. geophys. Res.,* **106,** 8887–8906.

Bercovici, D., Ricard, Y. & Schubert, G., 2001b. A two-phase model of compaction and damage. 3. Applications to shear localization and plate boundary formation, *J. geophys. Res.,* **106,** 8925–8940.

Blundy, J. & Cashman, C., 2001. Ascent-driven crystallisation of dacite magmas at Mount St Helens, 1980–1986, *Contrib. Mineral. Petrol.,* **140,** 631–650.

Campbell, I. & Pitcher, A., 1958. Shock waves in a liquid containing gas bubbles, *Proc. R. Soc. Lond. Ser. A,* **243,** 534–545.

Chojnicki, K., Clarke, A. & Phillips, J.C., 2006. A shock-tube investigation of the dynamics of gas-particle mixtures: implications for explosive volcanic eruptions, *Geophys. Res. Lett.,* **33,** doi:10.1029/2006GL026414.

Crighton, D. & Williams, J.F., 1969. Sound generation by turbulent two-phase flow, *J. Fluid Mech.,* **36,** 385–603.

Crowe, C., Troutt, R. & Chung, J., 1996. Numerical models for two-phase turbulent flows, *Annu. Rev. Fluid Mech.,* **28,** 11–43.

Crowe, C., Sommerfeld, M. & Tsuji, Y., 1998. *Multiphase Flows with Droplets and Particles,* CRC-Press, Boca Raton, Florida.

Drew, D., 1971. Averaged field equations for two-phase media, *Stud. Appl. Math.,* **50,** 133–166.

Drew, D., 1983. Averaged field equations for two-phase flow, *Annu. Rev. Fluid Mech.,* **15,** 261–291.

Drew, D. & Passman, S., 1999. Theory of Multicomponent Fluids, *Appl. Math. Sci. Vol. 135*, Springer-Verlag, New York.

Drew, D. & Segel, L., 1971. Averaged equations for two-phase flows, *Stud. Appl. Math.,* **50,** 205–257.

Gonnermann, H.M. & Manga, M., 2007. The fluid mechanics inside a volcano, *Annu. Rev. Fluid Mech.,* **39,** 321–356.

Hier-Majumder, S., Ricard, Y. & Bercovici, D., 2006. Role of grain boundaries in magma migration and storage, *Earth planet Sci. Lett.,* **248,** 735–749.

Jaupart, C. & Tait, S., 1990. Dynamics of eruptive phenomena, *Rev. Mineral. Geochem.,* **24,** 213–238.

John, J., 1969. *Gas Dynamics,* Allyn and Bacon Inc., Boston.

Kaminski, E. & Jaupart, C., 1998. The size distribution of pyroclasts and the fragmentation sequence in explosive volcanic eruptions, *J. geophys. Res.,* **103,** 29 759–29 779.

Kaye, G. & Laby, T., 1972. *Tables of Physical and Chemical Constants,* Longman, New York.

Kieffer, S., 1977. Sound speed in liquid-gas mixtures: Water-air and water-stream, *J. geophys. Res.,* **82,** 2895–2904.

Kozono, T. & Koyaguchi, T., 2009a. Effects of relative motion between gas and liquid on 1-dimensional steady flow in silicic volcanic conduits: 1. an analytical method, *J. Volc. Geotherm. Res.,* **180,** 21–36.

Kozono, T. & Koyaguchi, T., 2009b. Effects of relative motion between gas and liquid on 1-dimensional steady flow in silicic volcanic conduits: 2. origin of diversity of eruption styles, *J. Volc. Geotherm. Res.,* **180,** 37–49.

Landuyt, W., Bercovici, D. & Ricard, Y., 2008. Plate generation and two-phase damage theory in a model of mantle convection, *Geophys. J. Int.,* **174,** 1065–1080.

Lockner, D., 1995. Rock failure, in *Rock Physics and Phase Relations: A Handbook of Physical Constants, AGU Ref. Shelf,* Vol. 3, pp. 213–238, ed. Ahrens, T.J., American Geophysical Union, Washington, DC.

Massol, H. & Jaupart, C., 1999. The generation of gas overpressure in volcanic eruptions, *Earth. planet. Sci. Lett.,* **166,** 57–70.

McKenzie, D., 1984. The generation and compaction of partially molten rock, *J. Petrol.,* **25,** 713–765.

Melnik, O.E., 2000. Dynamics of two-phase conduit flow of high-viscosity gas-saturated magma: large variations of sustained explosive eruption intensity, *Bull. Volc.,* **62,** 153–171.

Melville, W. & Bray, K., 1979. A model of the two-phase turbulent jet, *Int. J. Heat Mass Transfer,* **22,** 647–656.

Michaut, C. & Bercovici, D., 2009. A model for the spreading and compaction of two-phase viscous gravity currents, *J. Fluid Mech.,* **630,** 299–329.

Michaut, C., Bercovici, D. & Sparks, R., 2009. Ascent and compaction of gas rich magma and the effects of hysteretic permeability, *Earth planet Sci. Lett.,* **282,** 258–267.

Mitchell, K., 2005. Couple conduit flow and shape in explosive volcanic eruptions, *J. Volc. Geotherm. Res.,* **143,** 187–203.

Morton, B., Taylor, G. & Turner, J., 1956. Turbulent gravitational convection from maintained and instantaneous sources, *Proc. R. Soc. Lond. Ser. A, Math. Phys. Sci.,* **234,** 1–23.

Ogden, D. & Wohletz, K., 2010. Ash particulate size and the formation of shock waves in volcanic jets, *Geophys. Res. Lett.,* submitted.

Ogden, D., Glatzmaier, G. & Wohletz, K., 2008a. Effects of vent overpressure on buoyant eruption columns: implications for plume stability, *Earth planet. Sci. Lett.,* **268,** 283–292.

Ogden, D., Wohletz, K., Glatzmaier, G. & Brodsky, E., 2008b. Numerical simulations of volcanic jets: importance of vent overpressure, *J. geophys. Res.,* **113,** B02204, doi:10.1029/2007JB005133.

Papale, P., 2001. Dynamics of magma flow in volcanic conduits with variable fragmentation efficiency and nonequilibrium pumice degassing, *J. geophys. Res.,* **106,** 11 043–11 065.

Pitsch, H., 2006. Large-eddy simulation of turbulent combustion, *Annu. Rev. Fluid Mech.,* **38,** 453–482.

Ricard, Y. & Bercovici, D., 2003. Two-phase damage theory and crustal rock failure: the theoretical 'void' limit, and the prediction of experimental data, *Geophys. J. Int.,* **155,** 1057–1064.

Ricard, Y., Bercovici, D. & Schubert, G., 2001. A two-phase model of compaction and damage, 2. applications to compaction, deformation, and the role of interfacial surface tension, *J. geophys, Res.,* **106,** 8907–8924.

Sparks, R.S.J., 1978. The dynamics of bubble formation and growth in magmas: a review and analysis, *J. Volc. Geotherm. Res.,* **3,** 1–37.

Spiegelman, M., 1993. Physics of melt extraction: theory, implications and applications, *Philos. Trans. R. Soc. Lond., Ser. A,* **342,** 23–41.

Sramek, O., Ricard, Y. & Bercovici, D., 2007. Simultaneous melting and compaction in deformable two-phase media, *Geophys. J. Int.,* **168,** 964–982.

Venkateswaran, S., Lindau, J.W., Kunz, R.F. & Merkle, C.L., 2002. Computation of multiphase mixture flows with compressibility effects, *J. Comput. Phys.,* **180,** 54–77, doi:10.1006/jcph.2002.7062.

Vergniolle, S. & Jaupart, C., 1986. Separated two-phase flow and basaltic eruptions, *J. geophys. Res.,* **91,** 12 842–12 860.

Walker, G., 1980. The Taupo pumice: product of the most powerful known (ultraplinian) eruption? *J. Volc. Geotherm. Res.,* **8,** 69–94.

Wallis, G., 1969. *One-Dimensional Two-Phase Flow,* McGraw-Hill, New York.

Wilson, L., 1976. Explosive volcanic eruptions–III. Plinian eruption columns, *Geophys. J. R. astr. Soc.,* **45,** 543–556.

Wilson, L., Sparks, R.S.J. & Walker, G.P.L., 1980. Explosive volcanic eruptions. IV. The control of magma properties and conduit geometry on eruption column behavior, *Geophys. J. R. astr. Soc.,* **63,** 117–148.

Witte, J.H., 1969. Mixing shocks in two-phase flow, *J. Fluid Mech.,* **36,** 639–655.

Woods, A., 1988. The fluid dynamics and thermodynamics of eruption columns, *Bull. Volc.,* **50,** 169–193.

Woods, A.W., 1995. The dynamics of explosive volcanic eruptions, *Rev. Geophys.,* **33,** 495–530.

Woods, A. & Bower, S., 1995. The decompression of volcanic jets in a crater volcanic eruptions, *Earth planet. Sci. Lett.,* **131,** 189–205.

Young, J.B. & Guha, A., 1991. Normal shock-wave structure in two-phase vapour-droplet flows, *J. Fluid Mech.,* **228,** 243–274.

Zhang, D.Z. & Prosperetti, A., 1994. Averaged equations for inviscid disperse two-phase flow, *J. Fluid Mech.,* **267,** 185–219.

APPENDIX A: INTERACTION FORCE ΔI

The interaction force between phases ΔI is due to flow only; the pressure and surface tension interaction has already been isolated and results in the terms proportionally to ω in eqs (4) and (5). The interaction force of one phase on the other is necessarily equal and opposite to the reverse force. In viscous flows ΔI amounts to Darcy drag (for flow through a permeable matrix) or Stokes drag (for motion of non-connected parcels of one phase through the other); in less viscous flow, this drag term needs to be adjusted for turbulent drag. Moreover, in low-viscosity flows, the interaction force involves inertial interchange due to one phase accelerating through the other (Drew 1971; Drew & Segel 1971; Drew 1983; Drew & Passman 1999; Zhang & Prosperetti 1994). Both of these interaction forces are discussed later.

A1 Interface drag

The viscous interface drag force is typically simply written as

$$\Delta I_d = c\Delta \mathbf{v}, \tag{A1}$$

where c is a drag coefficient. We can divide c into viscous/laminar and turbulent drag components c_v and c_t, respectively.

For viscous or laminar Darcy drag on fluid percolating through a permeable matrix (with interconnected fluid pathways), c_v is related to fluid phase viscosity μ_g and matrix permeability k, such that $c_v \sim \mu_g/k$. Alternatively for Stokes drag with non-interconnected phases, like droplets or particles passing through the surrounding medium, c is related to the surrounding medium viscosity and the characteristic droplet/particle size r; in the case of magma particles of radius r travelling through gas $c_v \sim \mu_g/r^2$.

The turbulent drag force scales as the Reynolds stress, but acts against phase separation, and thus appears as $\Delta I_{td} = c_t\Delta \mathbf{v} = c_v\Gamma v_e\Delta \mathbf{v}$ where $c_v\Gamma$ depends on the density of the turbulent medium and the characteristic size of particles travelling through it (Section A1.1), and v_e is an effective eddy velocity scale. Because the direction of this drag force is only determined by $\Delta \mathbf{v}$ then v_e should be positive definite as well as Galilean invariant, for which an obvious candidate is $v_e = \sqrt{\Delta \mathbf{v} \cdot \Delta \mathbf{v}} = |\Delta \mathbf{v}|$, which states that the eddy transport depends on the kinetic energy of relative motion between phases. Therefore, the net interface drag is postulated to be

$$\Delta I_d = (c_v + c_t)\Delta \mathbf{v} = c_v(1 + \Gamma|\Delta \mathbf{v}|)\Delta \mathbf{v}, \tag{A2}$$

where this defines $c_t = c_v\Gamma|\Delta \mathbf{v}|$; recall that ΔI_d applies to the gas phase momentum, while $-\Delta I_d$ applies to the magma phase momentum.

A1.1 A simple interface drag model

To estimate the form of various terms in eq. (A2), we follow the concepts of Michaut & Bercovici (2009) and consider a spherical magma particle of radius r and density ρ_m moving under its own buoyancy through a mixture of gas and other particles at a vertical velocity Δw relative to the gas. Assuming the particle reaches terminal velocity, the force balance on it is

$$0 = -\frac{4}{3}\pi r^3(\rho_m - \overline{\rho})g - 4\pi r^2 \mu_g \Delta w/r - 4\pi r^2 \rho_g |\Delta w|\Delta w,$$
(A3)

where the buoyancy term (first term on the left side) is for the particle density relative to an effective mixture density (i.e. an Archimedian compensation accounting for the hydrostatic pressure fields induced by other buoyant or heavy particles), and the other two terms account for viscous drag of the gas (proportional to gas viscosity μ_g) and turbulent drag of the gas (proportional to the effective Reynolds traction of the gas $\rho_g |\Delta w|\Delta w$). Given that the mixture density $\overline{\rho} = \phi \rho_g + (1 - \phi)\rho_m$ then the force balance (A3) becomes

$$0 = -\phi \Delta \rho g - \frac{3}{r}\left(\frac{\mu_g}{r} + \rho_g|\Delta w|\right)\Delta w.$$
(A4)

Allowing for particle buoyancy relative to the mixture (rather than gas) density partially accounts for the effects of non-dilute suspensions; that is particles interact through the fluid (gas) phase by pressure variations, which we assume are, to leading order, due to the weight of particles. This assumption is of course violated at very high particle velocities, where dynamic pressures due to particle motion as well as particle spin (which induces aerodynamic lift) are significant (see Crowe *et al.* 1998); however, in this analysis such velocities occur near the choking point where the porosity is approaching unity and the mixture is a very dilute suspension.

The two-phase mixture equations in theory capture the same scenario: in particular, the vertical component of ϕ times (5) minus $(1 - \phi)$ times (4) in the limit of steady uniform flow and properties, leads to

$$0 = -\phi(1 - \phi)\Delta \rho g - c\Delta w,$$
(A5)

where $\Delta \boldsymbol{I} \cdot \hat{\mathbf{z}} = c\Delta w$ for the uniform steady case. Comparing (A4) and (A5) leads to an expression for the total effective drag coefficient $c = c_v + c_t$, that is

$$c = \frac{3(1 - \phi)\mu_g}{r^2}\left(1 + \frac{\rho_g r|\Delta w|}{\mu_g}\right),$$
(A6)

where the factor $\rho_g r|\Delta w|/\mu_g$ is of course the Reynolds number for the particle moving through the gas. In this regard, c_v and Γ from (A2) are given by

$$c_v = 3(1 - \phi)\mu_g/r^2$$
(A7)

$$\Gamma = \rho_g r/\mu_g.$$
(A8)

We will, however, adopt the more general form for the interface drag coefficient relevant for dispersed particles:

$$c = \overline{c}(1 - \phi)(1 + \Gamma|\Delta \mathbf{v}|),$$
(A9)

where $\overline{c} = 3\mu_g/r^2$.

A2   Inertial exchange

In low-viscosity flows, the interaction force involves inertial interchange due to one phase accelerating through the other (Drew 1971;

Drew & Segel 1971; Drew 1983; Drew & Passman 1999; Zhang & Prosperetti 1994). The most common effect of such exchange is the virtual mass (or added mass) effect wherein a small particle accelerating through a fluid gains extra inertia equal to $\frac{1}{2}$ the displaced mass of fluid; for example an accelerating parcel of magma with mass $\rho_m dV$ gets an effective mass of $(\rho_m + \frac{1}{2}\rho_g)dV$.

Another consequence of inertial exchange is the Basset force, which treats the 'history' effect of a lagging viscous boundary layer on a particle accelerating through a fluid (Basset 1961). In essence, the mass of fluid in a viscous boundary layer accelerated in the wake of a particle of size r scales as $\delta_v(t)r^2\rho_g$, where $\delta_v = \sqrt{\mu_g t/\rho_g}$ is the viscous boundary layer length. The Basset force is not necessarily negligible (although commonly neglected in two-phase literature; Drew & Passman (1999), chap. 18) and may be important relative to standard inertia and virtual mass for increasingly small particle sizes (given the dependence on r^2 rather than r^3) and/or sufficiently long time scales. However, given the implied integro-differential complexity (i.e. a time integral over particle history up to a time t to get the force at that time), we here neglect this force, which thus assumes intermediate particle sizes and/or short time scales. Development of the theory with this force is, however, worthy of future considerations.

Considerable literature exists on the form of the inertial interaction force. Drew (1971) (see also Drew & Segel 1971; Drew & Passman 1999; Zhang & Prosperetti 1994) advocated an objectively invariant form, that is independent of reference frame even if accelerating. However, their proposed form lacks symmetry between the two equations and is thus not materially invariant (Bercovici *et al.* 2001a), and thus cannot capture, for example, the virtual mass effect in both limits of $\phi \to 1$ and $\phi \to 0$. Moreover, the priority for objective invariance for this force is arguable because the interaction is not due to viscous stresses (which are associated with deformation, and thus are not dependent on any reference frame, rotating or otherwise) but due to acceleration of phases through each other, hence should be affected by a non-inertial reference frame (e.g. a particle in a rotating frame of reference will accelerate through fluid if it moves toward or away from the rotation axis, as expected in the Coriolis effect).

Here we seek an interaction force that includes inertial interchange that has the proper material symmetry and captures the virtual mass effect in both limits of ϕ big and small. One can gain some insight as to the form of this relation by considering that, during inertial interchange, total momentum is conserved and thus the momentum imparted by one phase to the other across the interface between phases is equal and opposite to the reverse exchange. The momentum (per unit of mixture volume) imparted to the magma by the volume of gas displaced by magma particles is $\mathbf{J}_{gm} = \rho_g(1 - \phi)(\mathbf{v}_g - \check{\mathbf{v}})$ where $\check{\mathbf{v}}$ is the effective interface velocity (i.e. the displaced gas imparts momentum to the magma if it is moving relative to the interface); likewise the momentum imparted to the gas by the volume of magma displaced by gas is $\mathbf{J}_{mg} = \rho_m\phi(\mathbf{v}_m - \check{\mathbf{v}})$. These increments in momentum are equal and opposite and thus add to 0, which provides an equation for the interface velocity

$$\check{\mathbf{v}} = \frac{\rho_m\phi\mathbf{v}_m + \rho_g(1 - \phi)\mathbf{v}_g}{\rho_m\phi + \rho_g(1 - \phi)}$$
(A10)

in which case the increments of momentum exchange are simply

$$\mathbf{J}_{mg} = -\mathbf{J}_{gm} = \check{\rho}\Delta \mathbf{v},$$
(A11)

where

$$\check{\rho} = \frac{\rho_g\rho_m\phi(1 - \phi)}{\rho_m\phi + \rho_g(1 - \phi)}$$
(A12)

is an effective interface density. Considering the effective interface velocity and density implied by this momentum exchange, we propose an inertial exchange interaction force (i.e. rate of momentum exchange) of the form

$$\Delta \boldsymbol{I}_i = \frac{1}{2}\check{\rho}\left(\frac{\partial \Delta \mathbf{v}}{\partial t} + \check{\mathbf{v}} \cdot \nabla \Delta \mathbf{v}\right), \tag{A13}$$

where the rate of exchange is dependent on the velocity difference $\Delta \mathbf{v}$, the advection of this momentum occurs on an interface with velocity $\check{\mathbf{v}}$ and an effective density $\check{\rho}$, and the factor of $1/2$ is included to capture the virtual mass effect. In particular, in the limit of $\phi \to 1$ we obtain $\check{\rho} \to \rho_g(1-\phi)$ and $\check{\mathbf{v}} \to \mathbf{v}_m$ and the virtual mass effect is recovered in eq. (5); that is the inertial interchange force contributes to the acceleration term on the left side of the equation to give an effective acceleration term of $(\rho_m + \frac{1}{2}\rho_g)(1-\phi)\frac{D_g \mathbf{v}_m}{Dt}$. The identical effect exists for the gas equation in the limit of small gas bubbles (i.e. $\phi \to 0$) in a low-viscosity magma.

A3 Total interaction force

Considering interface drag and inertial exchange we propose the net interaction force

$$\Delta \boldsymbol{I} = \bar{c}(1-\phi)(1+\Gamma|\Delta\mathbf{v}|)\Delta\mathbf{v} + \frac{1}{2}\check{\rho}\left(\frac{\partial \Delta \mathbf{v}}{\partial t} + \check{\mathbf{v}} \cdot \nabla \Delta \mathbf{v}\right). \tag{A14}$$

APPENDIX B: ENERGY CONSERVATION

The total energy of the two-phase mixture in a volume δV is

$$E = \int_{\delta V}\left[\rho_g \phi\left(\frac{1}{2}v_g^2 + \varepsilon_g\right) + \rho_m(1-\phi)\left(\frac{1}{2}v_m^2 + \varepsilon_m\right) + \xi \Theta\right]dV, \tag{B1}$$

where ε_g and ε_m are the specific internal energies of the gas and magma phase, ξ is the full surface energy on the interface and Θ is the interfacial area density (interface area per unit volume). As discussed in Bercovici *et al.* (2001a), the interface surface energy is comprised of a reversible work component equivalent to the surface tension σ, and a part involving surface entropy, which for single component systems is equivalent to $-d\sigma/dT$ where T is temperature, assumed the same in both phases at any given point in space (i.e. local thermal equilibrium); that is

$$\xi = \sigma - T\frac{d\sigma}{dT}. \tag{B2}$$

If this is a fixed open volume, then the rate of change of E is given by the flux of energy through the surface δA of the volume by advective and non-advective transport, the rate of work done by forces exerted on the volume from outside, and internal energy sources:

$$\frac{\partial E}{\partial t} = -\int_{\delta A}\rho_g\left(\frac{1}{2}v_g^2 + \varepsilon_g\right)\mathbf{v}_g \cdot \hat{\mathbf{n}}\phi\, dA$$
$$-\int_{\delta A}\rho_m\left(\frac{1}{2}v_m^2 + \varepsilon_m\right)\mathbf{v}_m \cdot \hat{\mathbf{n}}(1-\phi)\, dA$$
$$-\int_{\delta A}\xi\Theta\tilde{\mathbf{v}}\cdot\hat{n}\, dA - \int_{\delta A}\mathbf{q}\cdot\hat{\mathbf{n}}\, dA + \int_{\delta V}Q\, dV$$
$$+\int_{\delta V}(\rho_g\phi\mathbf{v}_g + \rho_m(1-\phi)\mathbf{v}_m)\cdot\mathbf{g}\, dV$$
$$-\int_{\delta A}P_g\mathbf{v}_g\cdot\hat{\mathbf{n}}\phi\, dA - \int_{\delta A}P_m\mathbf{v}_m\cdot\hat{\mathbf{n}}(1-\phi)\, dA, \tag{B3}$$

where $\tilde{\mathbf{v}} = \omega\mathbf{v}_g + (1-\omega)\mathbf{v}_m$ is the effective velocity at which interface energy is transported; in (Bercovici & Ricard 2003) ω is inferred to be weighted by viscosity and prescribes the effective bulk viscosity, as is relevant for viscous phases; in this model of effectively inviscid phases, we are free to select ω such that $\tilde{\mathbf{v}} = \check{\mathbf{v}}$.

The energy conservation law is reduced by substituting (B1) and (B2) into (B3), applying Green's integral theorem to the surface integrals, extracting rates of change of density and porosity with the mass conservation eqs (1) and (2), and eliminating kinetic energy terms with the inner product between the phase velocities $\mathbf{v}_g$ and $\mathbf{v}_m$ with their respective momentum equations (4) and (5). This eventually yields

$$\rho_g\phi\frac{D_g\varepsilon_g}{Dt} + \rho_m(1-\phi)\frac{D_m\varepsilon_m}{Dt} - T\frac{\tilde{D}}{Dt}\left(\Theta\frac{d\sigma}{dT}\right)$$
$$-T\Theta\frac{d\sigma}{dT}\nabla\cdot\tilde{\mathbf{v}} = \Delta\mathbf{v}\cdot\Delta\boldsymbol{I} - \left(\Delta P\frac{\tilde{D}\phi}{Dt} + \sigma\frac{\tilde{D}\Theta}{Dt}\right)$$
$$+\frac{P_g}{\rho_g}\frac{D_g\rho_g}{Dt} + Q - \nabla\cdot\mathbf{q}, \tag{B4}$$

where

$$\frac{\tilde{D}}{Dt} = \frac{\partial}{\partial t} + \tilde{\mathbf{v}}\cdot\nabla = \omega\frac{D_g}{Dt} + (1-\omega)\frac{D_m}{Dt}. \tag{B5}$$

The melt phase is assumed incompressible, which implies that $d\varepsilon_m = Td\mathcal{S}_m$, and the gas phase is compressible such that $d\varepsilon_g = Td\mathcal{S}_g - P_g d(1/\rho_g)$, where $\mathcal{S}_m$ and $\mathcal{S}_g$ are the magma and gas specific entropies, respectively. As there is no viscous resistance to compaction (because the magma components are low viscosity and are not in contact) under the pressure difference ΔP, then the mechanical work done by the interface pressure drop $-\Delta P\frac{\tilde{D}\phi}{Dt}$ is exactly balanced by work done by surface tension $\sigma\frac{\tilde{D}\Theta}{Dt}$, and the second term on the right side of (B4) is zero; as discussed in Bercovici *et al.* (2001a), if $\Theta = \Theta(\phi)$ then this balance is equivalent to Laplace's surface tension condition $\Delta P = -\sigma\frac{d\Theta}{d\phi}$. If we further neglect surface tension with $\sigma = 0$, then $\Delta P = 0$ meaning there is only one pressure, $P_m = P_g$. For further simplicity, we also neglect any internal heat production (i.e. $Q = 0$) and bulk conductive or radiative cooling ($\mathbf{q} = 0$).

The above various assumptions taken together yield

$$\rho_g\phi T\frac{D_g\mathcal{S}_g}{Dt} + \rho_m(1-\phi)T\frac{D_m\mathcal{S}_m}{Dt} = \Delta\mathbf{v}\cdot\Delta\boldsymbol{I}. \tag{B6}$$

Because the melt phase is assumed incompressible, we can further write $Td\mathcal{S}_m = c_m dT$. Assuming the gas phase is ideal, then we repose the gas entropy with $Td\mathcal{S}_g = d\varepsilon_g + P_g d(1/\rho_g)$ in which $\varepsilon_g = \frac{\nu}{2}\frac{R}{m_g}T = c_g T$ and $P_g/\rho_g = \frac{R}{m_g}T$ where ν is the number of degrees of freedom (e.g. 3 for monatomic gas, 5 for diatomic, etc.). These assumptions transform (B6) into

$$\phi c_g\rho_g T\frac{D_g}{Dt}\left(\log\frac{T}{\rho_g^{2/\nu}}\right) + (1-\phi)\rho_m c_m\frac{D_m T}{Dt} = \Delta\mathbf{v}\cdot\Delta\boldsymbol{I}. \tag{B7}$$

Finally, we employ (7) to write

$$\phi c_g\rho_g T\frac{D_g}{Dt}\log\left(\frac{T}{\rho_g^{2/\nu}}\right) + (1-\phi)\rho_m c_m\frac{D_m T}{Dt}$$
$$= c\Delta v^2 + \frac{1}{4}\check{\rho}\frac{\check{D}\Delta v^2}{Dt}, \tag{B8}$$

where $\frac{\check{D}}{Dt} = \frac{\partial}{\partial t} + \check{\mathbf{v}}\cdot\nabla$. The term proportional to $\check{\rho}$ is not positive definite, thus it cannot by itself be an entropy source. However, it represents non-dissipative kinetic energy exchange between phases

by the virtual mass effect that might otherwise be counted as turbulent dissipation. Thus, this term can be considered the *reversible exchange* correction to dissipation by turbulent drag. Because the turbulent drag goes as $\bar{c}\Gamma\Delta v^3 \sim (\rho_g/r)\Delta v^3$ (where r is particle size; see A8) it should be much larger in magnitude than the virtual mass energy exchange which goes as $\rho_g \check{\mathbf{v}} \cdot \nabla \Delta v^2$, since r is much much smaller than the length scale for gradients in Δv^2.

In the absence of substantive frictional heat input due to phase separation (i.e. assuming it is negligible relative to the initial sensible heat), the eruption is largely isentropic, in which case the entropy equation becomes

$$\frac{D_g}{Dt}\log\left(\frac{T}{\rho_g^{2/\nu}}\right) + \frac{(1-\phi)\rho_m c_m}{\phi c_g \rho_g}\frac{D_m \log T}{Dt} = 0. \tag{B9}$$

In the post-fragmentation eruption column, the gas fraction ϕ is significant and thus ϕ is comparable to 1. However, $\rho_m \gg \rho_g$ (and the heat capacities are of comparable magnitude) thus the second term on the left side of (9) dominates (unless $\phi \to 1 - \rho_g/\rho_m$ such that the mixture becomes roughly 99 per cent gas by volume), which means that the eruption is predominantly isothermal, i.e. the temperature is buffered by the large heat capacity per volume ($\rho_m c_m$) of the magma. Therefore, we will assume that the system is predominantly isothermal and temperature T is hereafter a constant, as assumed in the main text.

APPENDIX C: SUPPLEMENTAL MATHEMATICAL ANALYSIS

C1 Linear acoustic-porosity waves

Perturbations in gas density and porosity to a two-phase erupting volcanic column, undergoing gravitational separation, will excite simultaneous acoustic and porosity waves. To illustrate the coupled wave dynamics of these disturbances, we examine a first-order linearized theory.

The general governing equations are (1)–(5), with (8) employed for the inter-phase drag. We assume a steady eruptive column, and consider perturbations in gas density ρ_g, porosity (gas fraction) ϕ and velocities w_g and w_m to this steady state; that is

$$\begin{aligned}
\phi &= \phi_0 + \epsilon\phi_1, \\
\rho_g &= \rho_0(1 + \epsilon\theta_1), \\
w_m &= w_{m0} + \epsilon w_{m1}, \\
w_g &= w_{g0} + \epsilon w_{g1},
\end{aligned} \tag{C1}$$

where subscript 0 denotes zeroth order steady background state, subscript 1 denotes first-order perturbation, and $\epsilon \ll 1$. We substitute these relations into the governing equations and consider solutions at zeroth and first order in ϵ.

C1.1 Zeroth order background state

The zeroth order solutions are assumed to be steady state, although not necessarily spatially uniform, especially ambient gas density ρ_0; however, we will find conditions under which the zeroth order state is approximately uniform.

The conservation of mass equation for the gas phase (1) becomes, to zeroth order in ϵ

$$\frac{\partial \rho_0 \phi_0 w_{g0}}{\partial z} = 0, \tag{C2}$$

which implies that

$$\frac{1}{\rho_0}\frac{\partial \rho_0}{\partial z} + \frac{1}{\phi_0 w_{g0}}\frac{\partial \phi_0 w_{g0}}{\partial z} = 0. \tag{C3}$$

As shown later, when considering zeroth order momentum equations, we can assume that $\frac{1}{\rho_0}\frac{\partial \rho_0}{\partial z}$ is negligible within a given height range and provided it is not multiplied by $\mathcal{C}_g^2$. This implies that $\phi_0 w_{g0}$ is approximately uniform, and assuming that ϕ_0 is constant then the background gas velocity w_{g0} is uniform also.

The conservation of mass for the magma phase (2) becomes, to zeroth order in ϵ

$$\frac{\partial(1-\phi_0)w_{m0}}{\partial z} = 0, \tag{C4}$$

which implies that w_{m0} is also uniform.

Because both zeroth order velocities are uniform, the conservation of momentum equations for both phases become, to $O(\epsilon^0)$

$$0 = -\phi_0 \mathcal{C}_g^2 \frac{\partial \rho_0}{\partial z} + \bar{c}(1-\phi_0)(1+\Gamma_0|\Delta w_0|)\Delta w_0 - \rho_0\phi_0 g, \tag{C5}$$

$$\begin{aligned}
0 = &-(1-\phi_0)\mathcal{C}_g^2\frac{\partial \rho_0}{\partial z} - \bar{c}(1-\phi_0)(1+\Gamma_0|\Delta w_0|)\Delta w_0 \\
&- \rho_m(1-\phi_0)g,
\end{aligned} \tag{C6}$$

where $\Gamma_0 = \rho_0 r/\mu_g$.

Adding eqs (C5) and (C6) yields

$$0 = -\mathcal{C}_g^2\frac{\partial \rho_0}{\partial z} - \bar{\rho}_0 g, \tag{C7}$$

where $\bar{\rho}_0 = \phi_0\rho_0 + (1-\phi_0)\rho_m$. The zeroth order gas density gradients are thus prescribed by

$$\frac{1}{\rho_0}\frac{\partial \rho_0}{\partial z} = \frac{\bar{\rho}_0 g}{\rho_0 \mathcal{C}_g^2}. \tag{C8}$$

The typical values of relevant parameters are $\rho_m \approx 2500\,\text{kg m}^{-3}$, $2\,\text{kg m}^{-2} \le \rho_0 \le 30\,\text{kg m}^{-3}$ from the top to the bottom of the column, $\phi_0 \approx 0.7$ and $\mathcal{C}_g \approx 700\,\text{m s}^{-1}$; therefore, $\frac{1}{\rho_0}\frac{\partial \rho_0}{\partial z} \approx 10^{-2} - 10^{-3}\,\text{m}^{-1}$, which means that variations in zeroth order density are negligible within length scales less than 1000 m. This appears a somewhat limiting condition, but really only means that perturbations propagating along the column will feel little effect from density stratification over increments in height under 1000 m. We thus consider perturbations propagating within such height increments and assume that variations and gradients in gas density are negligible unless multiplied by $\mathcal{C}_g^2$.

The steady-state zeroth order separation velocity is inferred by taking the weighted difference between momentum equations, i.e. $\phi_0 \times$(C6) $-(1-\phi_0)\times$(C5) which yields

$$0 = -\bar{c}(1+\Gamma_0|\Delta w_0|)\Delta w_0 - \phi_0 \Delta\rho_0 g, \tag{C9}$$

where $\Delta\rho_0 = \rho_m - \rho_0$. It is clear from (C9) that $\Delta w_0 < 0$ and thus the solution for it is

$$\Delta w_0 = \frac{1}{2\Gamma_0} - \sqrt{\left(\frac{1}{2\Gamma_0}\right)^2 + \frac{\Delta\rho_0 g\phi_0}{\bar{c}\Gamma_0}}. \tag{C10}$$

Given that $\bar{c} = 3\mu_g/r^2$, $\Gamma_0 = \rho_0 r/\mu_g$, and with typical values of gas viscosity $\mu_g \approx 10^{-5}\,\text{Pa s}$ and particle size $10^{-4}\,\text{m} \le r \le 10^{-2}\,\text{m}$, then $(2\Gamma_0)^{-2} \ll \Delta\rho_0 g\phi_0/(\bar{c}\Gamma_0)$. Thus, we can safely assume

$$\Delta w_0 = -\sqrt{\frac{\Delta\rho_0 g\phi_0}{\bar{c}\Gamma_0}} = -\sqrt{\frac{\Delta\rho_0 g\phi_0 r}{\rho_0}} \approx 0.2 - 10\,\text{m s}^{-1}. \tag{C11}$$

C1.2 First-order perturbation equations

To first order in ϵ the mass conservation equations are

$$\frac{D_g^0(\phi_1 + \phi_0\theta_1)}{Dt} + \phi_0\frac{\partial w_{g_1}}{\partial z} = 0, \tag{C12}$$

$$\frac{D_m^0\phi_1}{Dt} - (1-\phi_0)\frac{\partial w_{m1}}{\partial z} = 0, \tag{C13}$$

where $\frac{D_g^0}{Dt} = \frac{\partial}{\partial t} + w_{g0}\frac{\partial}{\partial z}$ and $\frac{D_m^0}{Dt} = \frac{\partial}{\partial t} + w_{m0}\frac{\partial}{\partial z}$.

The first-order momentum equations become, after some algebra,

$$\rho_0\phi_0\frac{D_g^0 w_{g_1}}{Dt} = -\rho_0\phi_0\mathcal{C}_g^2\frac{\partial\theta_1}{\partial z} + \Delta\rho_0 g\phi_1$$
$$- 2\Delta\rho_0 g\phi_0(1-\phi_0)\frac{\Delta w_1}{\Delta w_0} + \frac{1}{2}\breve{\rho}_0\frac{\breve{D}^0\Delta w_1}{Dt}, \tag{C14}$$

$$\rho_m(1-\phi_0)\frac{D_m^0 w_{m1}}{Dt} = -\rho_0(1-\phi_0)\mathcal{C}_g^2\frac{\partial\theta_1}{\partial z} + \rho_m g(1-\phi_0)\theta_1$$
$$+ 2\Delta\rho_0 g\phi_0(1-\phi_0)\frac{\Delta w_1}{\Delta w_0} - \frac{1}{2}\breve{\rho}_0\frac{\breve{D}^0\Delta w_1}{Dt}, \tag{C15}$$

where $\frac{\breve{D}^0}{Dt} = \frac{\partial}{\partial t} + \breve{w}_0\frac{\partial}{\partial z}$, $\breve{\rho}_0$ and $\breve{w}_0$ are $\breve{\rho}$ and $\breve{w}$ evaluated with ρ_0, ϕ_0, w_{g0} and w_{m0} according to (A10) and (A12); we also use the identities that $\mathcal{C}_g^2(\partial\rho_0/\partial z) = -\overline{\rho}_0 g$ (eq. C7) and that $\bar{c}\Gamma_0\Delta w_0^2 \approx \phi_0\Delta\rho_0 g$ (see eq. C9, with $\Gamma|\Delta w_0| = -\Gamma\Delta w_0 \gg 1$).

We next take a Galilean transformation of the perturbation equations to a frame of reference moving with the averaged ambient velocity $\overline{w}_0$. In this frame of reference gas moves at velocity $w_{g0} - \overline{w}_0 = -(1-\phi_0)\Delta w_0$ while magma particles move at velocity $w_{m0} - \overline{w}_0 = \phi_0\Delta w_0$. We also define dimensionless velocities ω_g, ω_m, height z' and time t' according to

$$(w_{g_1}, w_{m1}) = |\Delta w_0|(\omega_g, \omega_m), \quad z = \frac{|\Delta w_0|^2}{g}z', \quad t = \frac{|\Delta w_0|}{g}t'. \tag{C16}$$

With the Galilean transformation and the non-dimensionalization, the governing perturbation equations become (dropping primes on t' and z')

$$\left(\frac{\partial}{\partial t} + (1-\phi_0)\frac{\partial}{\partial z}\right)(\phi_1 + \phi_0\theta_1) + \phi_0\frac{\partial\omega_g}{\partial z} = 0, \tag{C17}$$

$$\left(\frac{\partial}{\partial t} - \phi_0\frac{\partial}{\partial z}\right)\phi_1 - (1-\phi_0)\frac{\partial\omega_m}{\partial z} = 0, \tag{C18}$$

$$\phi_0\left(\frac{\partial}{\partial t} + (1-\phi_0)\frac{\partial}{\partial z}\right)\omega_g = -\alpha^2\phi_0\frac{\partial\theta_1}{\partial z} + \beta_m\phi_1$$
$$+ 2\beta_m\phi_0(1-\phi_0)\Delta\omega + \frac{1}{2}(1-\phi_0)\left(\frac{\partial}{\partial t} - \phi_0\frac{\partial}{\partial z}\right)\Delta\omega, \tag{C19}$$

$$\beta_m(1-\phi_0)\left(\frac{\partial}{\partial t} - \phi_0\frac{\partial}{\partial z}\right)\omega_m = -\alpha^2(1-\phi_0)\frac{\partial\theta_1}{\partial z}$$
$$+ \beta_m(1-\phi_0)\theta_1 - 2\beta_m\phi_0(1-\phi_0)\Delta\omega$$
$$- \frac{1}{2}(1-\phi_0)\left(\frac{\partial}{\partial t} - \phi_0\frac{\partial}{\partial z}\right)\Delta\omega, \tag{C20}$$

where $\alpha = \mathcal{C}_g/|\Delta w_0|$ and, as defined earlier, $\beta_m = \rho_m/\rho_0$; moreover, in writing these dimensionless equations we acknowledge for

simplicity that $\rho_m \gg \rho_0$ such that $\beta_m \gg 1$ and $\breve{\rho}_0 \approx \rho_0$ and $\breve{w}_0 = w_{m0}$ (or in dimensionless, Galilean transformed coordinate $\breve{\omega}_0 = -\phi_0$).

We next assume a sinusoidal wave structure to the perturbations whereby

$$\phi_1, \theta_1, \omega_g, \omega_m \sim e^{ik(z-\mathcal{C}t)}. \tag{C21}$$

However, to simplify the math and eliminate ϕ_0 due to gas and magma advective velocities, we define $\mathcal{C} = \frac{1-2\phi_0-\mathcal{Y}}{2}$. Substitution of these solution forms into (C17)–(C20) yields after extensive algebra,

$$0 = k^2\frac{(\mathcal{Y}-1)^2}{4}\left(\frac{\alpha^2\phi_0}{1-\phi_0} + \frac{\mathcal{Y}^2-1}{8} - \frac{(\mathcal{Y}+1)^2\phi_0}{4(1-\phi_0)}\right)$$
$$+ \beta_m((1-\phi_0)\mathcal{Y} + 2 - 3\phi_0)$$
$$+ ik\left(\frac{\phi_0(\mathcal{Y}+1)}{4}\left[\beta_m(\mathcal{Y}-1)^2 + \frac{(\mathcal{Y}+1)(\mathcal{Y}+1-2\phi_0)}{1-\phi}\right]\right.$$
$$\left. - \alpha^2\frac{\mathcal{Y}+2-3\phi}{1-\phi} + \frac{\mathcal{Y}^2-1}{8}\right), \tag{C22}$$

which can be recast as a fourth order polynomial relation for $\mathcal{Y}$ as given by eq. (42), the solutions of which are discussed in the main text.

C2 Non-linear steady-state numerical solutions

The governing equations to the 1-D steady-state system are described by eq. (44). To facilitate numerical analysis, we define the dimensionless dynamic pressure of the magma particles as

$$\mathcal{P} = \beta_m(1-\phi_0)^2/(1-\phi) \tag{C23}$$

in which case eq. (44b) simply becomes

$$\frac{d\mathcal{P}}{dz} = -\bar{\alpha}^2(1-\phi)\frac{d\theta}{dz} - \beta_m(1-\phi) - \Delta\mathcal{I}, \tag{C24}$$

where $\Delta\mathcal{I}$ is given by eq. (45). Eq. (44) can be added together to obtain the net mixture momentum equation in 1-D:

$$\frac{d\Pi}{dz} = -(\theta\phi + \beta_m(1-\phi)) \tag{C25}$$

where

$$\Pi = \mathcal{P} + \frac{\phi_0^2}{\theta\phi} + \bar{\alpha}^2\theta \tag{C26}$$

is the total dimensionless (dynamic plus thermodynamic) pressure of the mixture. In this way our dependent variables become $\mathcal{P}$ and Π, and ϕ and θ are functions of these new variables such that

$$\phi(\mathcal{P}) = 1 - \beta_m(1-\phi_0)^2/\mathcal{P} \tag{C27}$$

and

$$\theta(\mathcal{P}, \Pi) = \frac{1}{2\bar{\alpha}^2}\left(\Pi - \mathcal{P} \pm \sqrt{(\Pi-\mathcal{P})^2 - 4\bar{\alpha}^2\phi_0^2/\phi(\mathcal{P})}\right). \tag{C28}$$

The root of eq. (C28) is chosen so that $\theta = 1$ when $\phi = \phi_0$; in this case the positive root is necessary for the most general case of $\phi_0 < \bar{\alpha}^2$. (This result is inferred by using eq. C26 to eliminate $\Pi - \mathcal{P}$ from eq. (C28) and substituting $\phi = \phi_0$ and $\theta = 1$ into the resulting expression to obtain the constraint that $1 = \frac{1}{2\bar{\alpha}^2}(\phi_0 + \bar{\alpha}^2 \pm |\phi_0 - \alpha^2|)$, which requires the positive root for $\phi_0 < \bar{\alpha}^2$.)

Eqs (C24) and (C25) are nominally the two governing ordinary differential equations. However, since eq. (C24) involves derivatives of functions of $\mathcal{P}$ and/or Π (such as θ and $\Delta\mathcal{U}$) then we need to repose the equation as

$$\frac{\mathrm{d}\mathcal{P}}{\mathrm{d}z} = \left[(\theta\phi + \beta_{\mathrm{m}}(1-\phi)) \left(\bar{\alpha}^2(1-\phi)\frac{\partial\theta}{\partial\Pi} + \frac{1}{2}\breve{\beta}\breve{\mathcal{U}}\frac{\partial\Delta\mathcal{U}}{\partial\Pi} \right) \right.$$
$$\left. - \beta_{\mathrm{m}}(1-\phi) - \mathcal{D}\Delta\mathcal{U} \right] \Bigg/$$

$$\left[1 + \bar{\alpha}^2(1-\phi)\frac{\partial\theta}{\partial\mathcal{P}} + \frac{1}{2}\breve{\beta}\breve{\mathcal{U}}\frac{\partial\Delta\mathcal{U}}{\partial\mathcal{P}} \right], \tag{C29}$$

where $\Delta\mathcal{U}$ and $\breve{\mathcal{U}}$ are given by eqs (46) and (47), respectively, and $\mathcal{D}$ is given by eq. (48). In this way, eqs (C25) and (C29) are the governing equations, with the boundary conditions that $\theta = \phi/\phi_0 = 1$ at $z = 0$; or alternatively that $\mathcal{P} = \beta_{\mathrm{m}}(1 - \phi_0)$ and $\Pi = \beta_{\mathrm{m}}(1 - \phi_0) + \phi_0 + \bar{\alpha}^2$ at $z = 0$.